J. Fluid Mech. (1989), *vol.* 199, *pp.* 297–332
Printed in Great Britain

Effects of heat release on the large-scale structure in turbulent mixing layers

By P. A. McMURTRY†, J. J. RILEY‡ AND R. W. METCALFE‖

† University of Utah, Salt Lake City, UT 84112, USA
‡ University of Washington, Seattle, WA 98195, USA
‖ University of Houston, Houston, TX 77004, USA

(Received 29 December 1987 and in revised form 1 June 1988)

The effects of chemical heat release on the large-scale structure in a chemically reacting, turbulent mixing layer are investigated using direct numerical simulations. Three-dimensional, time-dependent simulations are performed for a binary, single-step chemical reaction occurring across a temporally developing turbulent mixing layer. It is found that moderate heat release slows the development of the large-scale structures and shifts their wavelengths to larger scales. The resulting entrainment of reactants is reduced, decreasing the overall chemical product formation rate. The simulation results are interpreted in terms of turbulence energetics, vorticity dynamics, and stability theory. The baroclinic torque and thermal expansion in the mixing layer produce changes in the flame vortex structure that result in more diffuse vortices than in the constant-density case, resulting in lower rotation rates of the large-scale structures. Previously unexplained anomalies observed in the mean velocity profiles of reacting jets and mixing layers are shown to result from vorticity generation by baroclinic torques.

1. Introduction

Many chemically reacting flows are turbulent and are characterized by large amounts of energy release, resulting in large density changes. If the Damköhler number of the flow is large (fast chemistry), the reaction rate will be controlled by molecular diffusion and fluid dynamical mixing. Properly treating the turbulent behaviour is then an essential part of any predictive method for this type of flow. In a diffusion flame within a turbulent mixing layer, for example, product formation is augmented by the stretching and wrinkling of the reaction zone. A highly strained flow field develops, which increases the area of the reaction surface and produces an increased diffusion of reactants to this zone. For reactions that are accompanied by large amounts of heat release, the fluid dynamics will be coupled to the chemistry through the non-homogeneous density field that results. The objective of this work is to investigate the effects of exothermic chemical reactions on the turbulent flow field and to explain these effects through an examination of the physical mechanisms that are involved.

To study this problem, direct numerical simulations of two- and three-dimensional turbulent mixing layers have been performed. An exothermic chemical reaction between initially unmixed chemical species contained in the two feed streams is included. A mixing layer is formed when two initially separated parallel flowing fluids of different velocities come into contact and mix (figure 1). The somewhat idealized free-shear flow without heat release has been extensively studied and has proven

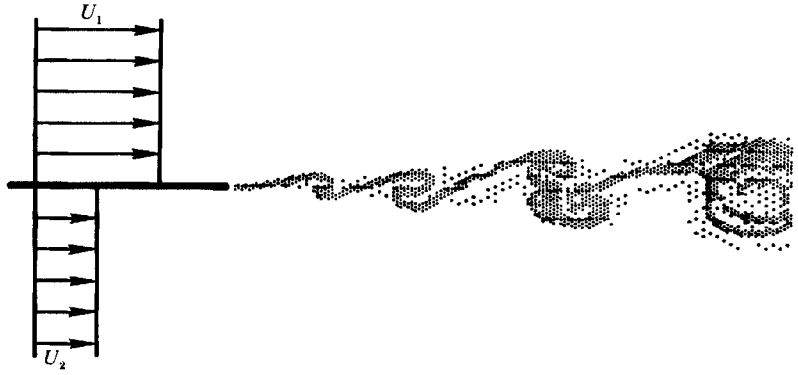

FIGURE 1. A schematic of the spatially developing mixing layer. Dots represent areas of vorticity concentration.

very useful in understanding turbulent flows. Laboratory experiments have shown that, at least in its early stages, the turbulent mixing layer is dominated by large-scale, quasi-two-dimensional vortices (Brown & Roshko 1974), with the growth of the mixing layer dominated by the pairing of these vortices (Winant & Browand 1974). Two-dimensional simulations have been shown to accurately portray the characteristic large-scale rollup and vortex-pairing processes (for example, Riley & Metcalfe 1980*b*; Aref & Siggia 1980; Patnaik, Sherman & Corcos 1976; Acton 1976). Implications of heat-releasing chemistry on this process can thus be addressed with two-dimensional simulations. Because all turbulent flows are inherently three-dimensional, some potentially important physics will be lost by restricting the simulations to two spatial dimensions. For example, secondary instabilities can develop into streamwise vortices or 'ribs' (Bernal 1981), which can increase mixing and enhance product formation. Three-dimensional simulations are necessary to study this type of behaviour and to realistically treat the turbulent behaviour of the flow.

There has been much work in the area of turbulent reacting flows with the objective of understanding the effects of the fluid dynamics on mixing and on reaction rates. A number of experiments have been performed on chemically reacting constant-density mixing layers to study the process of mixing and entrainment (Konrad 1976; Breidenthal 1981; Koochesfahani 1984; Mungal & Dimotakis 1984; Masutani 1985; Lasheras, Cho & Maxworthy 1986). In these experiments the chemistry had no influence on the development of the velocity field owing to the small amount of heat released. The results of these studies consistently showed that chemical-reaction products were concentrated in large, spanwise-coherent structures that, at least initially, dominate the turbulent transport. In addition, three-dimensional effects were present and found to be important. Breidenthal noted a significant increase in product formation rate coinciding with the development of three-dimensional motions in the flow. The experiments of Lasheras *et al.* investigated the origin and development of three-dimensional streamwise vorticity and showed that it substantially contributed to the entrainment process in the early stages of mixing-layer development.

Previous direct numerical simulations of a temporally evolving, incompressible reacting mixing layer (Riley, Metcalfe & Orszag 1986) focused on how the turbulent flow field affects the transport of chemical species. The simplified problem of a temperature-independent, single-step, chemical reaction without heat release was

used. This work has given physical insight into how vortex rollup and three-dimensional turbulence affect the chemical reaction. Despite the approximations used in the simulations, comparisons of these results with laboratory data have led to an increased confidence in the application of the direct numerical simulation methodology to chemically reacting flows. Givi, Jou & Metcalfe (1986) performed simulations of a temporally evolving reacting mixing layer and modelled the reaction rate with a more realistic one-step Arrhenius model. This model allowed them to study the effects of strain on the extinction of the flame. Their simulations showed that high strain rates are generated in the braids between adjacent vortices and that extinction can occur in these high-strain regions, in agreement with earlier asymptotic studies (Peters 1983). A constant-density flow was assumed so there was no influence of the chemistry on the velocity field.

Experimental studies undertaken to specifically investigate effects of heat release in turbulent reacting mixing layers have been performed by Wallace (1981) and Hermanson (1985). Wallace used a nitric oxide–ozone reaction to attain temperature rises of 400 K. Hermanson used a hydrogen–fluorine reaction to produce temperature rises to 940 K. Large-scale structures were observed to persist over these temperature ranges. All results obtained in these experiments indicated that the heat release resulted in a slower growth rate of the layer and a decrease in the total amount of mass entrained into the layer. Hermanson suggested that the decrease in mass entrainment could be attributed to a reduction in the turbulent shear stresses that were observed in the high-heat-release experiments. In both sets of experiments the streamwise pressure gradients were small. Hermanson performed additional experiments while imposing a favourable streamwise pressure gradient. These experiments showed an additional thinning of the layer.

Higher-heat-release experiments have been performed by Keller & Daily (1985), although under conditions different than in the experiments of Wallace and Hermanson. Cold premixed reactants carried in a high-velocity stream were ignited by hot, low-density combustion products which were in the low-speed stream. Results were reported for a range of equivalence ratios. In these experiments a large, favourable pressure gradient existed in the streamwise direction. The mixing-layer thickness was observed to increase with increasing heat release, a result different from what Hermanson and Wallace reported in their experiments with a diffusion-limited reaction and uniform upstream density. The thickening of the layer with heat release was attributed to the downstream acceleration of the low-speed, low-density fluid. Large-scale, two-dimensional vortices were again observed to persist over all heat-release ranges.

Visual studies of diffusion flames in jets (Whol, Gazley & Kapp 1949; Hottel & Hawthorne 1953; Takeno & Kotani 1975) have shown that the existence of flames (heat release) retards the transition from laminar to turbulent flow. More recent schlieren photographs of cold jets and attached jet flames by Savaş & Gollahalli (1986) and Gollahalli *et al.* (1986) clearly show the coherent structures near the jet exit are suppressed in the presence of flames. Turbulence measurements by Takagi, Shin & Ishio (1980) and Yule *et al.* (1981) show lower turbulence levels near the exit in jets with flames and an increase in turbulence downstream. Velocity profiles are steeper in the heat-release runs and Yule *et al.* report humps (more than one inflexion point) in the profiles that are not seen in the profiles for cold jets. Also, the frequencies of the most energetic instabilities (vortices at the fuel–air interface) were observed to decrease as heat release increased.

Numerical studies directed at isolating effects of heat release in reacting flows were

initiated by McMurtry *et al.* (1986) by performing direct numerical simulations of a two-dimensional temporally growing mixing layer undergoing exothermic chemical reactions. A low-Mach-number approximation was used which allowed the study of density change effects while eliminating the numerical stability requirements for computing the high-frequency acoustic waves. Although a temperature-independent reaction rate was employed, the fluid dynamics and chemistry were truly coupled in this work. The action of the baroclinic torque and thermal expansion was analysed to interpret the effects of heat release on the flow observed in the simulations and also in the experiments of Wallace and Hermanson.

Some theoretical work performed by Marble & Broadwell (1977) and Karagozian (1982) was helpful in interpreting the results of our simulations. Marble & Broadwell studied the deformation of a constant-density diffusion flame by turbulent motions. Karagozian examined the deformation of laminar diffusion flames in the flow field of two- and three-dimensional vortex structures, and also studied the effects of heat release on a laminar diffusion flame interacting with an inviscid vortex. The presence of density changes in the core caused the entire flow field to be shifted radially outward. The braids, or 'flame arms' of the vortex were thus translated to a region of lower total straining (further from the point where the vortex was imposed), reducing the rate at which reactants were consumed by the flame.

These previous investigations have demonstrated that there can be a very significant influence of combustion on the velocity field in reacting flows. The objective in our work is to use the simulation results of full three-dimensional chemically reacting mixing layers to better understand the mechanisms that produce these observed heat-release effects.

2. Methodology

Performing numerical studies specifically directed at investigating the basic interactions between the chemistry and the fluid dynamics calls for an approach in which the fundamental physical processes are an inherent part of the methodology. The approach used in this work is termed direct numerical simulation and involves solving the three-dimensional, time-dependent governing equations for the detailed development of the flow field (including the chemistry). This method of studying the nature and physics of turbulent flows was developed by Orszag & Patterson (1972) and was first applied to homogeneous turbulence. This technique uses no closure modelling so that no assumptions are made pertaining to the turbulent behaviour of the fluid. Direct numerical simulations can supplement laboratory experiments well and have the advantage that they can give much more detailed information about the flow, since the entire flow field is known at every time step. In particular, properties that are difficult or impossible to measure experimentally can often be obtained and studied in the simulations. In addition, initial conditions are easily controlled, and flow-field parameters can readily be varied to study their effect on the flow. Unfortunately, computer time and storage requirements limit the range of temporal and spatial scales that can be resolved, restricting full simulation to flows with moderate Reynolds and Damköhler numbers (although the latter limitation can be removed using a conserved scalar in the infinite-reaction-rate limit).

Because most laboratory experiments have been performed at higher Reynolds and Damköhler numbers than we are able to fully simulate numerically (owing to resolution limitations), it is not possible to precisely predict and quantitatively reproduce all details seen in laboratory experiments. However, the Reynolds number

imposed in our simulations is sufficiently high that the flow is turbulent (see §7), and many features observed in experiments also occur at the lower Reynolds numbers in our simulations. The simulations therefore provide a means to carefully examine the dynamics and evolution of these phenomena. Direct numerical simulation has been applied successfully in many recent studies of fluid dynamics. Reviews and examples of previous work addressing general turbulent flows can be found in Rogallo & Moin (1984), while a review of the application to reacting flows is contained in Jou & Riley (1989).

3. Numerical method

The results presented in the following sections are obtained from numerical simulations of a temporally growing mixing layer. This is not the same flow as the spatially developing layer that is usually studied experimentally, but is similar if the spatial layer is observed in a reference frame moving at the mean velocity. By studying a temporally growing layer, the requirement of specifying inflow–outflow boundary conditions, which are difficult to correctly implement for the spatial layer, is avoided. Furthermore, the amount of computer resources needed to obtain equivalent resolution is significantly greater for the spatially growing layer (Lowrey & Reynolds 1986). Because there are many dynamical features common to the two mixing layers (Metcalfe *et al.* 1987), a study of a temporal mixing layer can reveal important information about the spatial layer. Differences do, however, exist between these two flows. In the spatially developing layer, events that occur downstream can induce changes in the flow field upstream whereas in the temporally growing layer obviously no event can effect the flow at previous times. Also, the spatially developing layer has no symmetries around any spanwise axis so that entrainment rates of fluid into the layer from the two streams will not necessarily be the same. These differences between the spatial and temporal mixing layer, and others are discussed in detail by Corcos & Sherman (1984) and Dimotakis (1986). As pointed out by Riley & Metcalfe (1980*b*), exact agreement is only expected in the limit as the velocity difference across the layer becomes small.

In the temporally developing mixing layer studied here, periodic boundary conditions are applied in the streamwise (x) and spanwise (z) directions. In the transverse (y) direction, a free-slip, adiabatic boundary condition is applied. With these boundary conditions, very accurate pseudospectral (collocation) numerical methods can be efficiently implemented (see Gottlieb & Orszag 1977 and Canuto *et al.* 1988 for a description of these methods). All dependent variables are expanded in Fourier series in the streamwise and spanwise directions. In the transverse direction a Fourier cosine series is used for all dependent variables except for the transverse velocity component, v, which is expanded in a Fourier sine series. Spatial derivatives are then computed by differentiating the series term by term. A second-order-accurate Adams–Bashforth time-stepping scheme is used to advance the equations in time.

The pseudospectral technique as implemented here exhibits very small phase errors and numerical diffusion compared to finite-difference techniques. The numerical errors are truncation errors due to the finite wavenumber cutoff and time-stepping errors. Care has been taken to minimize these errors by using small time steps and adjusting transport coefficients (viscosity, molecular-diffusion coefficients) to be large enough to ensure accurate resolution. The lack of phase and diffusion errors is a very desirable property in simulations of reacting flows, where steep

gradients of reacting species can develop and where reaction rates are controlled by molecular diffusion. Truncation errors can become significant however, if gradients become too steep. A series of numerical experiments performed to assess the accuracy of the pseudospectral method in treating reacting flows is described by Riley *et al.* (1986).

4. Flow-field initialization

The computational domain for the simulations is chosen to be large enough to contain the most unstable mode and its subharmonic (as determined from linear stability theory for an incompressible flow (Michalke 1964)). The velocity field is initialized by adding a hyperbolic tangent velocity profile (figure 2) to a low-amplitude, three-dimensional, spectrally broadbanded background perturbation. To specify the background perturbation we use a method similar to that introduced by Orszag & Pao (1974) and discussed in detail in Riley & Metcalfe (1980*a*). Energy is assigned to each wavenumber component as specified by a selected three-dimensional energy spectrum. A random phase is then given to each component which results in a random velocity field with a specified energy spectrum. Simulations performed using various initial energy spectra, including white noise, indicated that the actual shape of the initial spectrum is not critical as long as energy is contained in a fairly wide range of wavenumbers. The spectrum used to initialize the turbulence in these simulations is given by

$$E_u(k) = \epsilon_{3d} \Lambda \frac{k^4 \Lambda^4}{(1+k^2\Lambda^2)^3}.$$

This is a fairly broadbanded, isotropic spectrum. Λ is the integral lengthscale, k is the wavenumber magnitude, and ϵ_{3d} is a coefficient that determines the level of the perturbation. The velocity field which has this spectrum is then multiplied by a 'form function' in physical space to give a turbulence intensity profile characteristic of mixing layers (Riley & Metcalfe 1980*b*). For simulations that start with a low enough initial amplitude, the most unstable frequencies will be selectively amplified.

The chemical reactant fields are initially one-dimensional and are given by the following functional relationships:

$$C_1(x,0) = \frac{1}{y_0 \pi^{\frac{1}{2}}} \int_{-\infty}^{y} \exp(-\zeta^2/y_0^2)\, \mathrm{d}\zeta,$$

$$C_2(x,y,z,0) = 1 - C_1(x, y+\delta, z, 0).$$

Here δ is a value by which the two species fields have been offset so that there is initially only a small region of overlap between the two (figure 2). These functions are easily resolvable using spectral methods and are not unlike those measured experimentally just downstream of the splitter plate in laboratory experiments. The particular chemical reaction used is the single step, irreversible reaction

$$C_1 + C_2 \rightarrow \text{Products} + \text{Heat}.$$

The reaction is a function only of the reactant concentrations and does not depend on temperature. Although some important features of real reacting flows are lost with this simple reaction, many important features of the effects of energy release on the dynamics of the flow can still be studied.

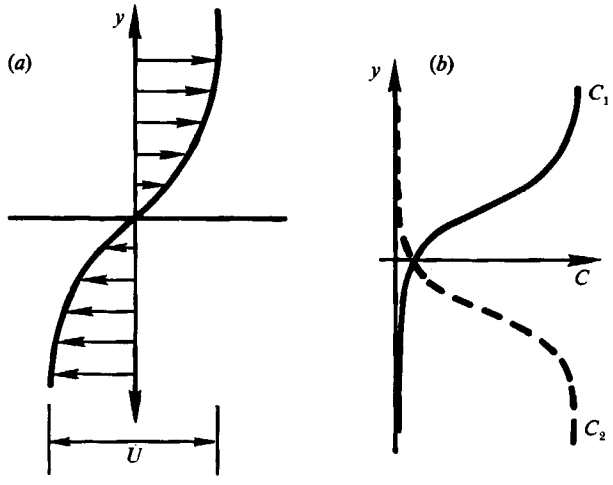

FIGURE 2. Initial (*a*) mean velocity and (*b*) mean chemical species profiles across the mixing layer.

5. Low-Mach-number approximation

To solve for the development of the flow field, a set of approximate equations valid for low-Mach-number flows (exact in the zero-Mach-number limit) is utilized. This approximation has previously been presented, in various forms, by Rehm & Baum (1978), Sivashinsky (1979), Buckmaster (1985), Majda & Sethian (1985), and McMurtry *et al.* (1986). The basic idea behind this approximation is that, for low-Mach-number flows, the acoustic waves generated by the turbulence and the combustion process have a much higher frequency and much faster propagation velocity than the motions characterizing convection processes. In addition, the energy in the acoustic waves is small compared both with the energy of the fluid convection velocity and to the thermodynamic internal energy. In the asymptotic limit as the Mach number goes to zero, the speed of sound becomes infinite and any disturbances in thermodynamic pressure will be felt instantaneously throughout the fluid. This approximation allows one to study effects of density changes due to heat release while filtering out the acoustic waves, thereby avoiding the numerical stability problems and resolution difficulties associated with computing acoustic-wave propagation.

Starting with the exact non-dimensional equations of combustion gas dynamics, then expanding each of the dependent variables in power series in the Mach number squared and equating coefficients of each power of the Mach number to zero, a set of ordered approximate equations is obtained. In this work, the equations solved include conservation equations for mass, momentum, energy, chemical species, and an equation of state. In the limit of zero Mach number, these equations take the following non-dimensional form (see McMurtry *et al.* 1986 for a detailed discussion and derivation of these equations):

$$\frac{\partial \rho^{(0)}}{\partial t} + \nabla \cdot \rho^{(0)} \boldsymbol{v}^{(0)} = 0, \tag{1a}$$

$$\nabla p^{(0)} = 0, \tag{1b}$$

$$\rho^{(0)} \frac{\mathrm{D}^{(0)}}{\mathrm{D}t} T^{(0)} = -(\gamma - 1) p^{(0)} \nabla \cdot \boldsymbol{v}^{(0)} + \frac{1}{PrRe} \nabla \cdot \boldsymbol{q}^{(0)} + Da\, Ce R_{\mathrm{p}}, \tag{1c}$$

$$\frac{\partial C_i^{(0)}}{\partial t} + \nabla \cdot C_i^{(0)} \boldsymbol{v}^{(0)} = Da R_i + \frac{1}{Pe} \nabla^2 C_i^{(0)}, \tag{1d}$$

$$p^{(0)} = \rho^{(0)} T^{(0)}. \tag{1e}$$

The momentum equation, to the lowest order (1*b*) simply imposes the spatial uniformity of the thermodynamic pressure $p^{(0)}$. To complete the description of the velocity field the first-order momentum equation must also be retained, and is given by

$$\rho^{(0)} \frac{\mathrm{D}^{(0)}}{\mathrm{D}t} \boldsymbol{v}^{(0)} = -\nabla p^{(1)} + \frac{1}{Re} \nabla \cdot \bar{\tau}^{(0)}. \tag{1f}$$

The non-dimensional parameters appearing in these equations are the Damköhler number, $Da = k_0 C_0 L_0 / U_0$, Péclet number, $Pe = L_0 C_0 / D_0$, and Reynolds number, $Re = U_0 L_0 / \nu$. The parameter Ce, a non-dimensional number characterizing the amount of heat release, is given by $Ce = C_0 \Delta H / \rho_0 C_v T_0$.

D_0, ν, C_0, ρ_0 and T_0 are the free-stream molecular diffusivity, kinematic viscosity, chemical species concentration per unit volume, density, and temperature. U_0 is the velocity difference across the layer, ΔH is the heat of reaction, k_0 is the reaction rate frequency, and C_v is the specific heat at constant volume. For computational convenience, the length-scale L_0 is chosen such that the non-dimensional wavelength of the most unstable mode (see §4) is $2\pi (2\pi = \lambda / L_0$, where λ is the dimensional wavelength). Time is non-dimensionalized by L_0 / U_0. Other variables appearing in (1*a–f*) include R_i, the reaction rate of the ith species, R_p, the rate of generation of product, and $\boldsymbol{q}$, the heat flux vector.

The distinction between the two pressures that appear, $p^{(0)}$ and $p^{(1)}$, is essential both from a theoretical point of view and in the numerical solution procedure. The thermodynamic pressure, $p^{(0)}$, is constant in space, but may vary in time owing to heat addition. $p^{(1)}$ is the dynamic pressure associated with the fluid motion and does not participate directly in thermodynamic processes.

These equations have previously been successfully applied to a two-dimensional problem (McMurtry *et al.* 1986). In that work, simulation results obtained using the exact compressible equations of motion with a free-stream Mach number of 0.2 were compared with simulation results using the low (zero)-Mach-number approximation. The impressive agreement between the two simulations confirmed the validity of the approximation in studying this type of flow. Other details of the numerical solution procedure are discussed elsewhere (McMurtry 1987).

6. Summary of approximations

The following is a summary of the major simplifications and approximations used in the numerical simulations.

(i) Low-Mach-number approximation. To ease stability requirements in the numerical calculations the low-Mach-number approximation is used. This allows acoustic waves to be filtered out of the equations. The validity of the approximation has been illustrated for these simulations by McMurtry *et al.* (1986) by comparing results obtained using the complete set of fully compressible flow equations with the results from the equations obtained from the low-Mach-number approximation.

(ii) Temporally developing mixing layer. The simulations are of a mixing layer that develops in time and is periodic in the streamwise and spanwise directions. As pointed out earlier, this is not the same flow as the spatially growing layer that is

usually encountered in practice. However, many dynamic similarities exist between the two so the temporally growing case is of relevance. Also, a more efficient and accurate computer code can be written for the temporally growing mixing layer for a given amount of computer resources.

(iii) Simple chemistry. A single step, irreversible reaction of the type A+B→ Products+Heat is used. The reaction is taken to be a function only of the reactant concentrations and does not depend on temperature. This chemical reaction is highly idealized, but allows the effects of chemical energy release in the flow to be studied.

(iv) Constant transport coefficients. The viscosity, thermal and molecular diffusivities, and the specific heats are taken to be temperature-independent constants. Again, this is not a realistic feature of general combusting flows, but, in addition to simplifying matters from a numerical point of view, it allows other effects on the flow to be isolated and studied in a simpler environment.

(v) Moderate heat release. This restriction is necessary to ensure the validity of the low-Mach-number approximation and can be understood by balancing terms in the exact, non-dimensional equations of motion (McMurtry *et al.* 1986). The condition that must be satisfied is $Da\,Ce = o(1)$. If $Da\,Ce \ll 1$, the equations will be valid, but the physics is uninteresting. On the other hand, additional terms must be kept in the expansion if $Da\,Ce \gg 1$. This does not, however, exclude fast chemistry. In the limit of infinite reaction rate, the overall heat generation and product formation can remain $o(1)$, since the concentration of reactants in the reaction zone become vanishingly small.

(vi) Finite wavenumber cutoff. The computations to be discussed in the following section were performed on a computational grid consisting of $64 \times 65 \times 64$ nodes. In the transformation to the wavenumber space this corresponds to computing the interactions of wavelengths consisting of wavenumbers $k_x, k_y, k_z = -32$ to 32, where k_x, k_y, k_z are the wavenumber vector components in the three coordinate directions.

7. Simulation results

Results are reported from simulations for two different values of the heat release parameter Ce: one with no heat release ($Ce = 0$, run 1), and the other giving a maximum density decrease of approximately $\rho/\rho_0 = 0.5$ ($Ce = 5$, run 2). These two simulations employ exactly the same initial velocity and species concentration fields. Other important non-dimensional parameters are the Reynolds, Péclet, and Damköhler numbers with values of 500, 500 and 2, respectively (defined in §5). The initial turbulence intensity was 4% of the velocity difference across the mixing layer. Additional simulations have been run using different random initial conditions. The results presented here are representative of all these runs.

Higher-heat-release cases than are presented here can be run, but, since the boundary conditions used here imply constant-volume combustion, the background pressure rises with time. Test cases with a computational domain twice as large in the transverse (y) direction were performed to verify that pressure rise effects due to the presence of the boundaries were not significant for the values of the parameters studied here.

Some aspects of the nature of the flow can be seen in a three-dimensional perspective plot of the total vorticity. In figure 3 surfaces having a value of 50% of the maximum of the sum of the absolute values of all three vorticity components are plotted ($|\omega_x| + |\omega_y| + |\omega_z| = \text{constant}$). This is a result from run 1 (initial random

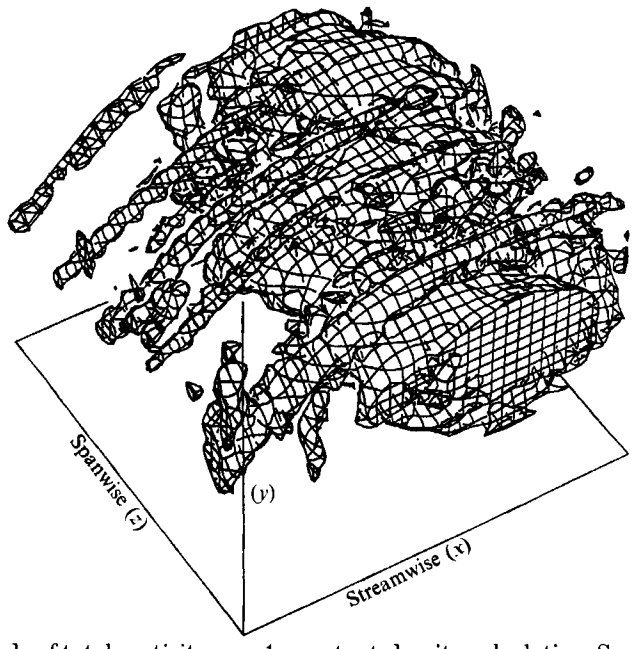

FIGURE 3. Magnitude of total vorticity, run 1, constant-density calculation. Surface plotted is 50% of the maximum vorticity level. Counter-rotating streamwise-oriented vorticity is characterized by the 'tubes' aligned in the x-direction.

velocity perturbations, no heat release). Clearly evident is the approximately two-dimensional spanwise vorticity structure associated with the rolling up of the mixing layer. These structures produce a stretching and wrinkling of the reaction interface that can lead to enhanced product formation (Riley *et al.* 1986; McMurtry *et al.* 1986). In addition, tubes aligned in the streamwise direction are also apparent. These structures, first observed by Konrad (1976) as streamwise streaks in a plan view of a gaseous mixing layer, were recognized to be counter-rotating vortices (Bernal 1981; Breidenthal 1981) and were subsequently modelled by Lin & Corcos (1984) and Pierrehumbert & Widnall (1982). The nature and evolution of these structures has since been studied in detail in the laboratory by Lasheras *et al.* (1986) and numerically by Metcalfe *et al.* (1987) and Ashurst & Meiburg (1988). The effect of these structures on the flow field is to induce a velocity field that acts to pump fluid between the two layers, thereby further convoluting the reaction interface. This tends to increase mixing between the two streams and enhance chemical reactions. One purpose of this work was to examine the influence of heat release on these processes and to study the influence this has on the product formation rate.

The effect of heat release on the chemical product formation for runs 1 and 2 is shown in figure 4, where the total product, i.e. the product concentration integrated over the entire computational domain

$$\frac{1}{V}\int\frac{C_{\mathrm{p}}}{C_0}\mathrm{d}V,$$

is plotted as a function of time. In agreement with previous two-dimensional results (McMurtry *et al.* 1986), the total product is seen to be lower for the case with heat release. Since the local instantaneous reaction rate is proportional to the product of the local species concentrations, this indicates that one effect of the heat release has

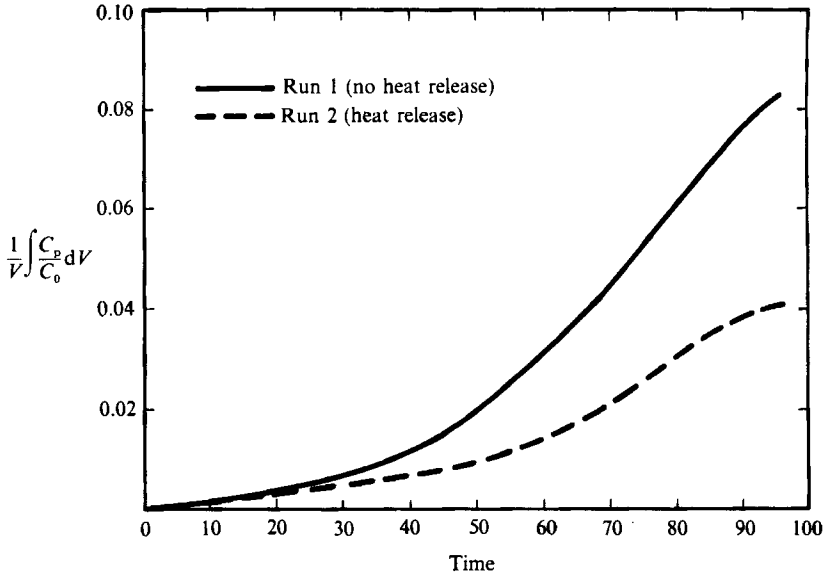

FIGURE 4. Total product formation as a function of time, run 1 (no heat release), run 2 (heat release). Curve plotted is the volume-averaged product mass fraction.

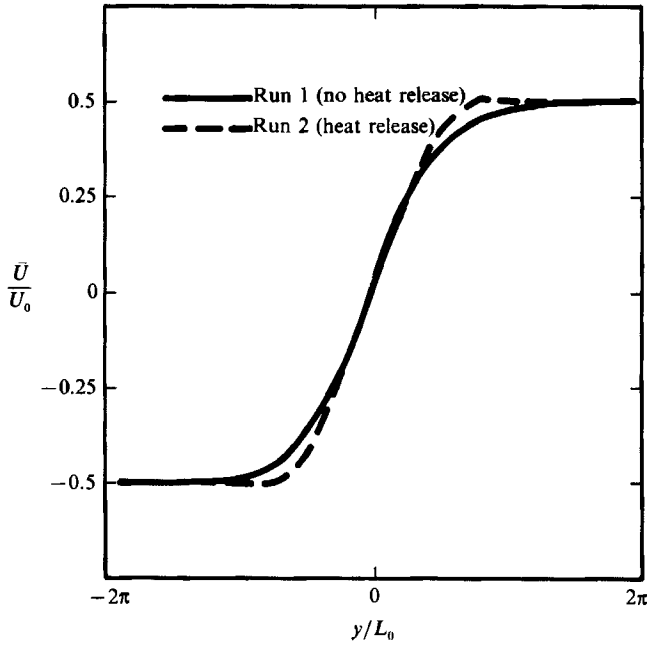

FIGURE 5. Velocity profile, run 1 (no heat release), run 2 (heat release), $t = 72$.

been to reduce the total amount of mixing between the two streams. An increase in the rate of product formation is seen to occur at about a time of 30 in the constant-density case (run 1) and at a time of 45 in the heat-release case. In both cases, this is due to the engulfment of fluid due to the rollup of the large-scale structures.

One measure of the layer growth is the vorticity thickness, defined as the ratio of the maximum velocity difference across the layer to the maximum slope of the mean velocity profile. The mean velocity profiles for runs 1 and 2 (figure 5) at a time of 72

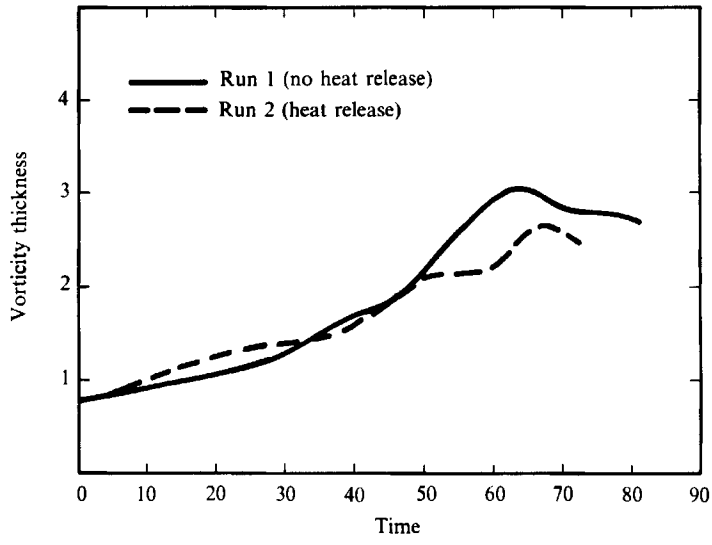

FIGURE 6. Vorticity thickness, run 1 (no heat release), run 2 (heat release).

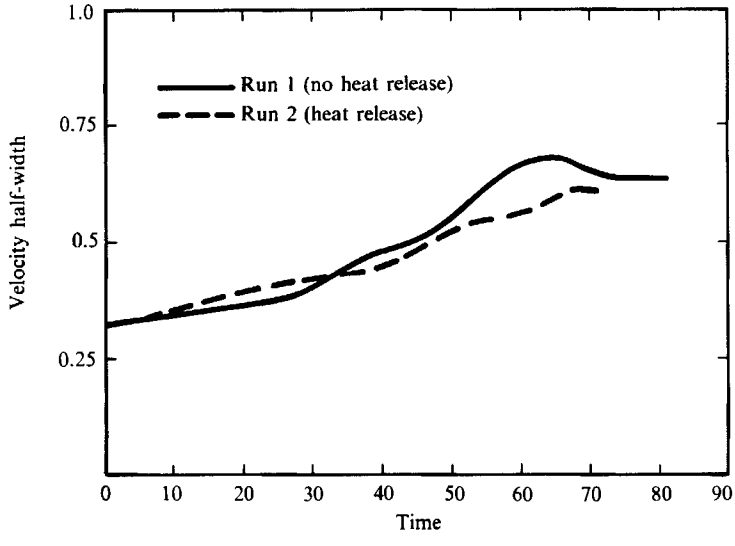

FIGURE 7. Velocity half-width, run 1 (no heat release), run 2 (heat release).

show a steeper profile for the heat release runs, indicating a slower rate of the layer growth. (Mean quantities are obtained by averaging over horizontal planes.) Note also the slight overshoot in the velocity profile that occurs in the heat-release run. These observations are similar to those obtained from previous two-dimensional calculations by McMurtry *et al.* (1986), which were initialized by adding the most unstable mode and its subharmonic to the mean flow. The overshoot in the velocity profile is not as pronounced in the three-dimensional simulations as in the two-dimensional ones. This is because of greater spanwise variation and lack of coherence that exists in the three-dimensional simulations. These overshoots seen in the velocity profile are similar to those observed in the jet flame experiments of Yule

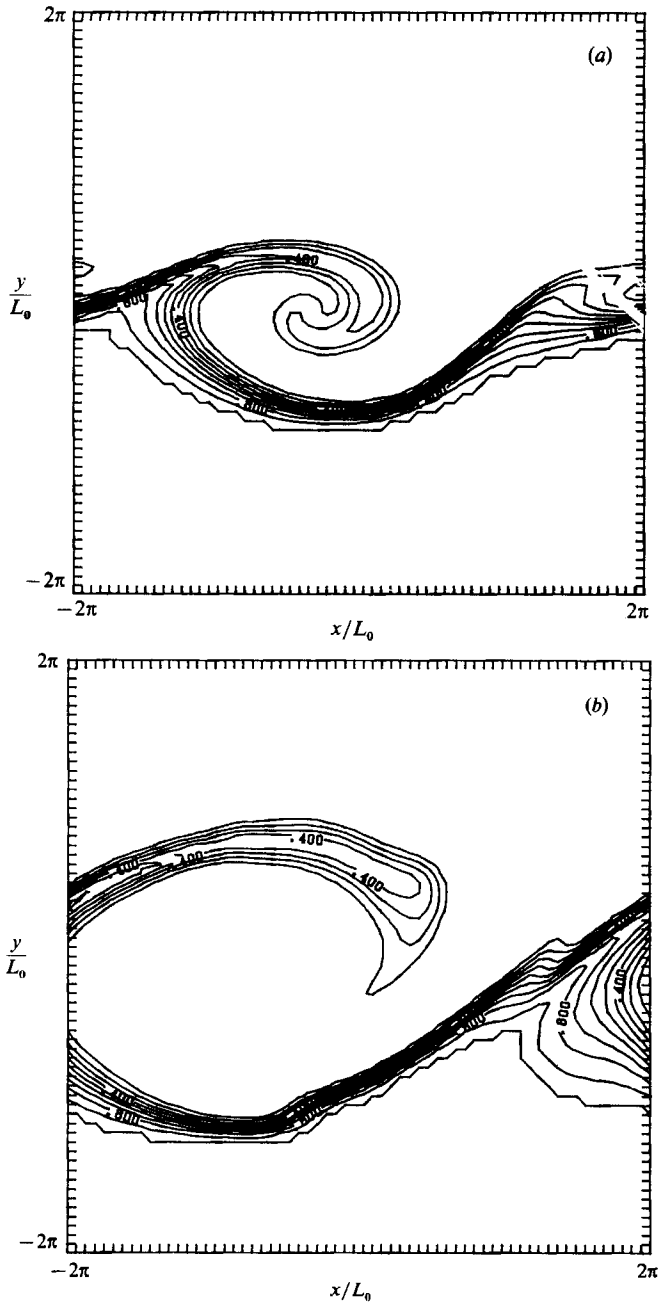

FIGURE 8. Contours of reacting-species concentration in one (x, y)-plane, no heat release. (*a*) $t = 48$; (*b*) $t = 72$. Contour level from 0 to 1.0.

et al. (1981) and have also been observed in reacting mixing layer experiments (M. G. Mungal 1986 and J. Hermanson 1986 private communications).

Plots of the vorticity thickness and velocity half-width (the lateral distance from the centreline of the mixing layer to the location where the average streamwise velocity component attains one half of its free-stream value) as a function of time reveal another interesting feature (figures 6 and 7). Initially, the growth of the layer

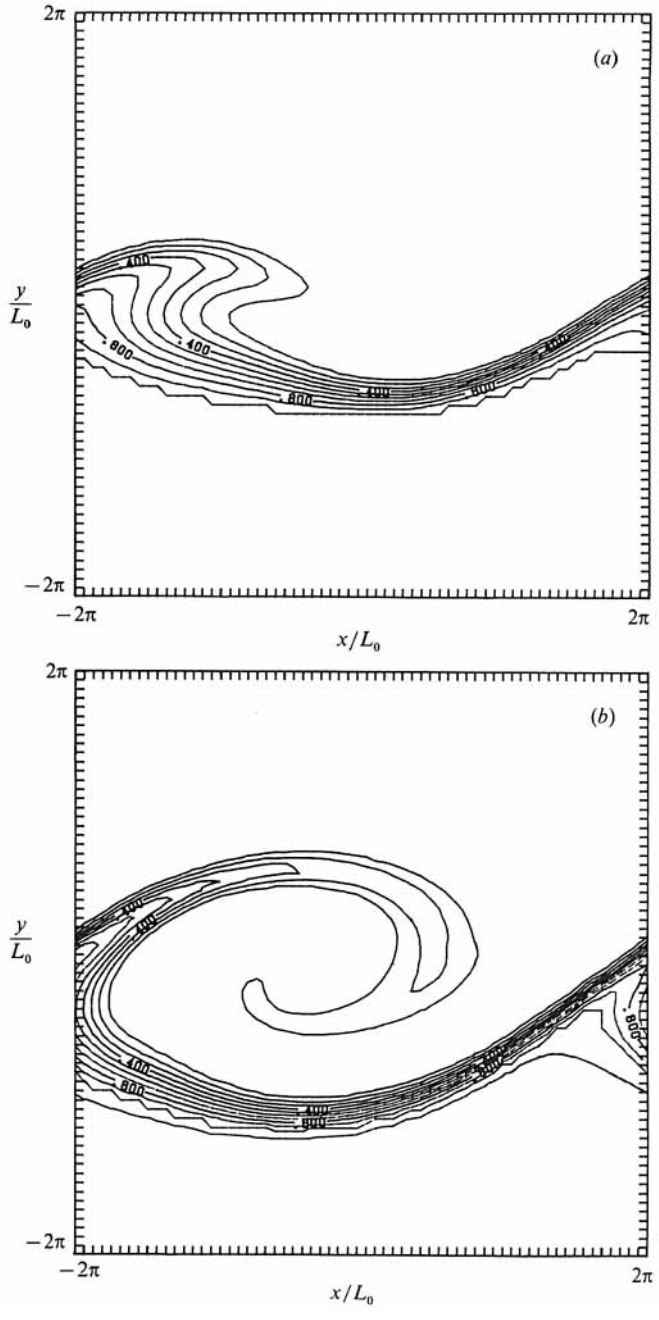

FIGURE 9. Contours of reacting-species concentration in one (x, y)-plane, with heat release. (a) $t = 48$; (b) $t = 72$. Contour level from 0 to 1.0.

given by these two measures is slightly greater in the heat-release case; this is true up to a time of about 30. At later times the layer thickness is less in the heat-release runs. The initial increase in the layer growth rate is a result of thermal expansion, which shifts the flow field in the vicinity of the reaction zone outward. Explanations for the smaller thickness seen in the heat-release runs at the later times are given in §10.

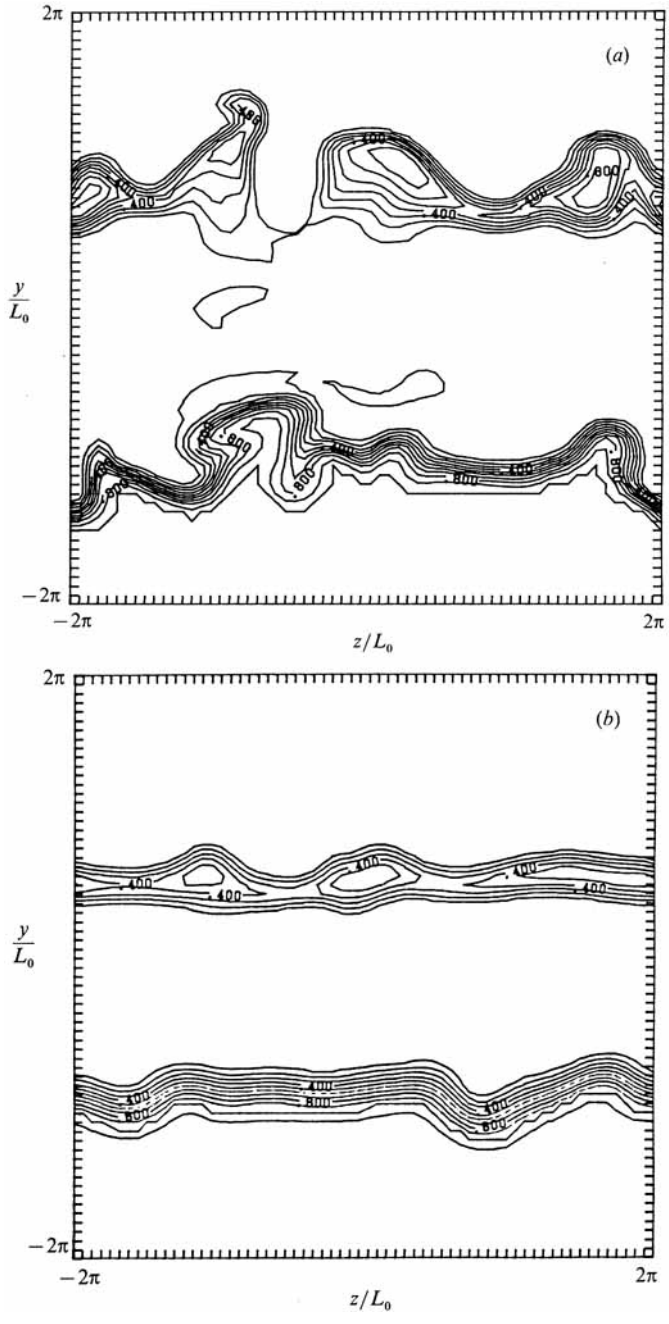

FIGURE 10. Contours of reacting-species concentration in the (y, z)-plane (plane perpendicular to mean flow), $t = 72$, contour level from 0 to 1.0. (*a*) No heat release; (*b*) with heat release.

A direct visualization of the chemical reactant fields further reveals some of these heat-release effects on the flow. Figures 8 and 9 are contour plots of one of the evolving chemical-species fields at the spanwise location $z = 0$. (This is one plane cut out of the three-dimensional flow field.) The large coherent structures in the flow are still apparent in the heat-release case. The initial rollup, however, appears to be inhibited as can be seen by a comparison between figures 8(*a*) and 9(*a*). The three-

dimensionality of the flow field is apparent in two-dimensional contour plots taken from cuts at different streamwise locations in the plane perpendicular to the mean flow. A (y, z)-plane through the core of the two-dimensional spanwise vortex is shown in figure 10. The mean flow direction is out of the page in the top half of the figure and into the page in the bottom half. Figure 10(*a*) is from the constant-density, no heat-release case while figure 10(*b*) is at the same location but for the heat-release case. The reactant field is clearly much less contorted in the heat-release case, indicating a stabilizing effect of heat release on the three-dimensional structures in the flow. This gives less surface area across which the chemical species can diffuse, resulting in part in the lower chemical-product formation rate seen in figure 4.

To summarize, the most obvious macroscopic effects of heat release on the mixing-layer dynamics revealed in these numerical simulations are a decrease in the product formation rate and, after a small initial increase, a decrease in the layer growth rate. These results are qualitatively similar to those obtained experimentally by Wallace (1981) and Hermanson (1985), and are consequences of lower rates of fluid entrainment into the mixing region when exothermic chemical reactions occur. In the following sections physical mechanisms responsible for these observations are suggested and described.

8. Turbulent stresses

It has been pointed out (Hermanson 1985) that most of the observed heat-release effects can be attributed to the decrease in the turbulent shear stresses. Velocity and density profiles obtained experimentally as well as the measured layer growth rate were used to compute the turbulent shear stress profiles in his experiments. In the numerical simulations performed here, it is possible to compute the turbulent shear stresses directly. The turbulent stresses are almost completely determined by the behaviour of the spanwise structures in our flow.

The computed Favre (density weighted)-averaged turbulent shear stress profiles $(\widetilde{\rho u_1'' u_j''})$ for runs with and without heat release are shown in figure 11. The wavy overbar denotes Favre-averaged quantities, which are defined as, e.g.

$$\tilde{U} = \frac{\overline{\rho u}}{\bar{\rho}}.$$

The fluctuating quantities are then given by

$$u'' = u - \tilde{U}.$$

The straight overbar refers to conventional Reynolds averaging. In the temporal calculations this is an average over a horizontal plane. It is well known that the turbulent stresses, $\widetilde{\rho u_k'' u_i''}$, represent a transport of mean momentum (per unit volume). In their Favre-averaged form these stresses include momentum exchange mechanisms due to turbulent transport, interactions between the mean flow and volumetric changes, and fluctuation–fluctuation interactions $(\overline{\rho' u_i' u_j'})$ (Libby & Williams 1981).

The suppression of the shear stress in the heat-release runs is clearly indicated. The lower turbulent stresses in the heat-release case imply a lower transport of momentum by the turbulence. This also indicates, as will be shown in the next section, that less energy is being transferred from the mean flow to the turbulence. In addition, the turbulent shear stresses can be directly related to the stability characteristics of the mixing layer, providing explanations for the lower growth rates of the mixing layer.

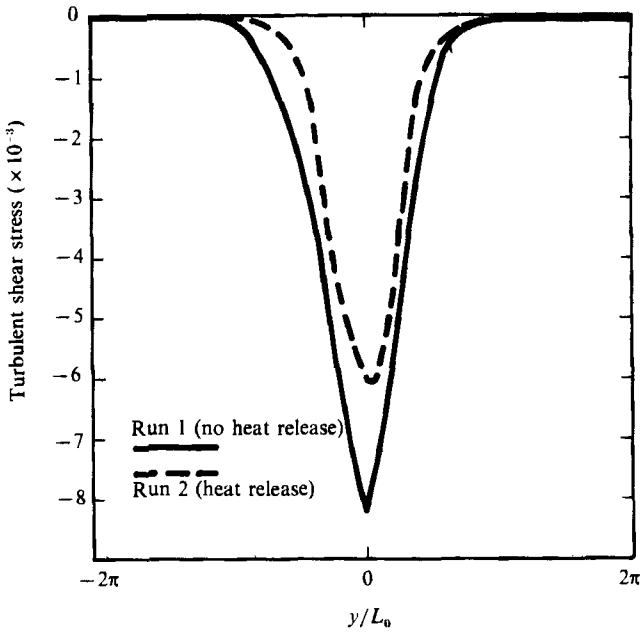

FIGURE 11. Favre-averaged turbulent shear stress profile, run 1 (no heat release), run 2 (heat release), $t = 48$.

9. Turbulent kinetic energy

Closely related to the turbulent shear stresses is the turbulent kinetic energy. Examination of the behaviour of the turbulent kinetic energy can provide a useful way to interpret the effects of heat release on the turbulent motions and to account for some of the observations in the heat-release runs. Furthermore, the turbulent kinetic energy and its production, redistribution, and viscous dissipation are important aspects of the flow that must be treated in many of the models currently used to describe turbulent flows.

The turbulent kinetic energy profile ($\frac{1}{2}\bar{\rho}\widetilde{u_i'' u_i''}$) for runs with and without heat release is shown in figure 12 at a non-dimensional time of $t = 48$. This corresponds to a time after the rollup of the most unstable mode and before the rollup of its subharmonic is complete. Again, these large-scale modes provide the dominant contribution to the turbulent kinetic energy. From this figure it can be seen that the total turbulent kinetic energy is less for the heat-release run. This is consistent with the earlier observations of less product formation and lower growth rates, since lower turbulence levels imply lower turbulent transport rates, resulting in a lower exchange of mass, momentum, and energy among fluid elements.

To understand how a lower turbulent kinetic energy profile results, it is useful to examine its transport equation. Written in Favre-average form, the transport equation for the turbulent kinetic energy is given by

$$\frac{\partial \bar{\rho} q}{\partial t} + \frac{\partial \tilde{U}_j \bar{\rho} q}{\partial x_j} = -\bar{\rho}\widetilde{u_k'' u_i''}\frac{\partial \tilde{U}_i}{\partial x_k} - \frac{\partial \bar{\rho}\widetilde{u_i'' u_i'' u_k''}}{\partial x_k} - \overline{u_i''\frac{\partial p'}{\partial x_i}} - \overline{\tau_{kl}\frac{\partial u_i''}{\partial x_k}},$$

where $q = \frac{1}{2}\widetilde{u_i'' u_i''}$ is the turbulent kinetic energy per unit mass.

The first term on the right-hand side describes the exchange of energy between the mean flow and the fluctuating motion. This production of kinetic energy is seen to

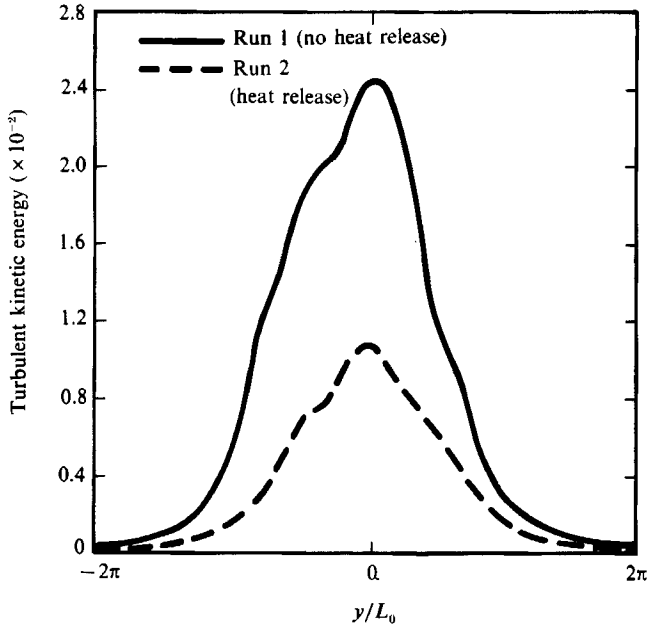

FIGURE 12. Turbulent kinetic energy profile, run 1 (no heat release), run 2 (heat release), $t = 48$.

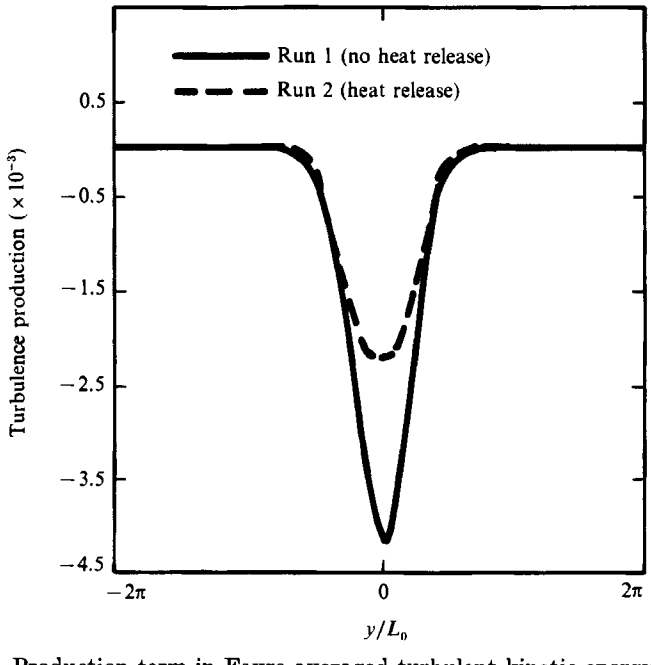

FIGURE 13. Production term in Favre-averaged turbulent kinetic energy equation, run 1 (no heat release), run 2 (heat release), $t = 48$.

be equal to the product of the mean velocity gradient and the turbulent stresses. In the mixing layer simulated here, the only non-zero contribution of this term is for $i = 1$ and $k = 2$. The profile of the turbulent production is shown in figure 13 at $t = 48$. Production is greatest at the centre of the mixing layer where the velocity gradient and turbulent stresses are the largest. (In the following plots, negative

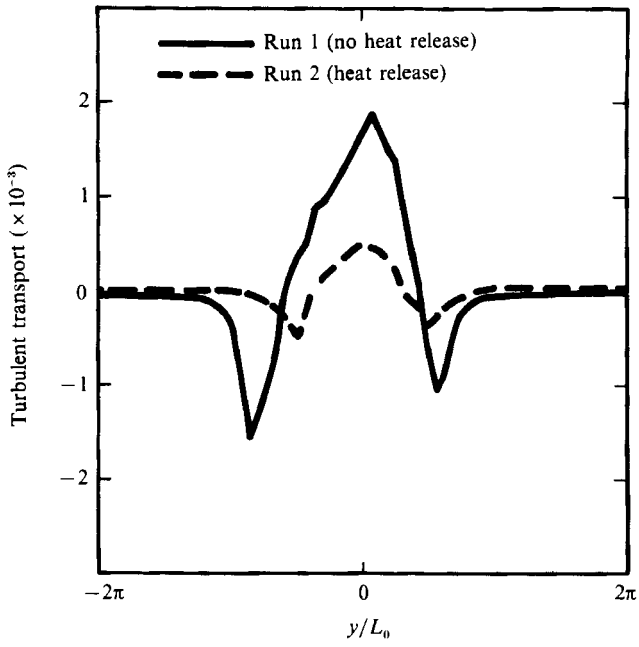

FIGURE 14. Turbulent transport term in kinetic energy equation, run 1 (no heat release), run 2 (heat release), $t = 48$.

values indicate a production of turbulent energy.) Although it was shown that the velocity gradient is steeper in the cases with heat release, the total turbulent kinetic energy production is less with heat release owing to the smaller turbulent stress term as shown in the previous section (figure 11). The velocity profile is plotted in figure 5.

The second term on the right is a conservative term and describes the redistribution of kinetic energy by the fluctuating velocity field. Figure 14 shows that turbulent transport tends to convect energy from the centre of the mixing layer, where the turbulent intensity is highest, to the outer regions. With the lower turbulence intensities that are seen in the heat-release runs, this term is of a lower magnitude in this case.

The effects of pressure fluctuations on the turbulent kinetic energy are described by the term $\overline{u_i'' \partial p'/\partial x_i}$. The value of this term is plotted in figure 15 at $t = 48$. This term is of the same order of magnitude as the production term, but has an opposite sign and does not appear to be as greatly affected by the heat release. The physical interpretation of this contribution can be clarified somewhat by writing it as

$$\overline{u_i'' \frac{\partial p'}{\partial x_i}} = \frac{\partial \overline{u_i'' p'}}{\partial x_i} - \overline{p' \frac{\partial u_i''}{\partial x_i}}.$$

The first term on the right-hand side is a conservative term describing the redistribution of kinetic energy by pressure fluctuations. The second term, which is zero for constant-density flows, is a source of kinetic energy resulting completely from the combustion. The contribution of these two terms for the heat-release run is shown in figure 16. The transport due to the pressure fluctuations is not much changed between the runs with and without heat release, although the peak magnitude is less in the heat-release runs. In both cases the pressure fluctuations act

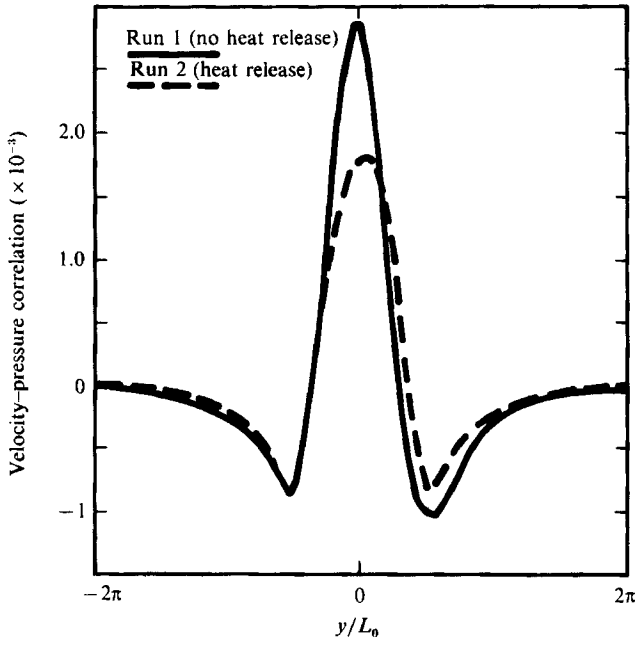

FIGURE 15. Velocity–pressure gradient correlation, run 1 (no heat release), run 2 (heat release), $t = 48$.

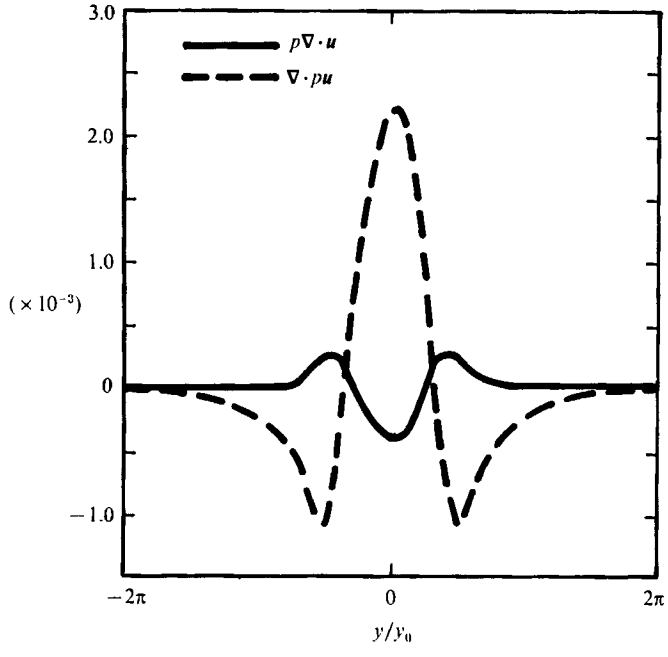

FIGURE 16. Contribution of expansion and pressure fluctuations to the velocity–pressure gradient correlation.

to transport energy away from the centre of the layer to the outer regions. The contribution due to the velocity divergence leads to an increase in kinetic energy at the centre of the vortices. In this respect the heat release acts to increase the turbulence level, although this effect is overshadowed by the decrease in the mean-flow production term.

From the results presented here, it is seen that the most significant effects of heat release on the turbulent kinetic energy balance are felt through the reduction in the mean-flow production of turbulent kinetic energy. A smaller contribution acting to increase the turbulence intensity is felt through the expansion part of the pressure gradient–velocity correlation. This production is, however, small in these simulations compared with the decrease in the mean-flow production term, yielding an overall lower turbulent kinetic energy profile. For higher rates of heat release, the term $\partial u_i''/\partial x_i$ would increase, resulting in more internal energy being converted to kinetic energy, and possibly, an overall increase in the turbulent kinetic energy.

10. Vorticity dynamics

Another approach to studying the flow and interpreting the effects of heat release on the flow field is in terms of vorticity dynamics. This allows a description of the flow directly in terms of the dynamics of the large-scale structures. In a two-dimensional flow without heat release or viscosity, the vorticity of a fluid particle is conserved, and the vorticity field can be used to directly visualize the flow field. In a three-dimensional flow, or a flow with density variations or expansion, this conservation property is no longer valid and hence the vorticity no longer serves as a reliable fluid marker. However, the dynamics of the flow field can still be understood and interpreted by studying the vorticity field.

In a general three-dimensional flow, the vorticity equation can be written in the following form:

$$\frac{\mathrm{D}\boldsymbol{\omega}}{\mathrm{D}t} = (\boldsymbol{\omega}\cdot\nabla)\boldsymbol{v} - \boldsymbol{\omega}(\nabla\cdot\boldsymbol{v}) + \frac{\nabla\rho\times\nabla p}{\rho^2} + \frac{1}{Re}(\nabla^2\boldsymbol{\omega}).$$

Four different mechanisms can be identified that alter the vorticity: vortex tube stretching and turning $(\boldsymbol{\omega}\cdot\nabla)\boldsymbol{v}$, thermal expansion, $\boldsymbol{\omega}(\nabla\cdot\boldsymbol{v})$, baroclinic torques, $(\nabla\rho\times\nabla p)/\rho^2$, and viscous diffusion. For a low-Mach-number flow without heat release, the expansion and baroclinic torque terms will be very small. When density changes due to heat release do occur, these two mechanism can be important in the vorticity dynamics.

The instantaneous spanwise component of vorticity (ω_3) at times of 48 and 72 is shown in figures 17 and 18 for runs 1 and 2. In the following figures dashed contour lines indicate negative vorticity (local rotation of fluid elements in the clockwise direction) and solid lines indicate positive vorticity. One of the most apparent differences between these two figures is that, for the simulations with heat release, the maximum amplitude of the vorticity, which occurs in the vortex cores, has decreased substantially. Furthermore, the vorticity is not as concentrated in the centre of the large structures as in the constant-density case. Also note the regions of positive-signed vorticity that appear at the outer edges of the vortex structures for the case with heat release. These reflect the generation of small eddies with a circulation opposite to that of the large spanwise structures.

As mentioned above, the mechanisms that produce the observed changes in the vorticity field in the heat-release runs are the baroclinic torques and thermal

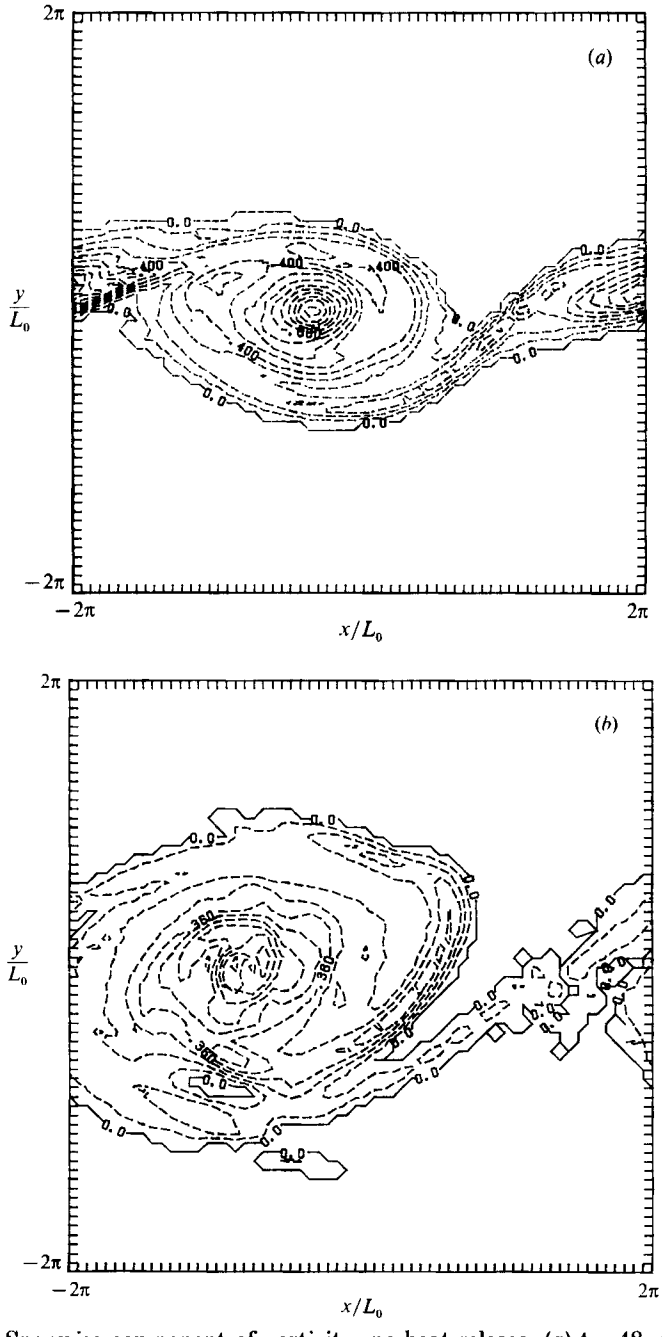

FIGURE 17. Spanwise component of vorticity, no heat release. (*a*) $t = 48$, contour level from -1.3 to 0. (*b*) $t = 72$, contour level from -0.9 to 0.

expansion. In an expanding flow, $\nabla \cdot \boldsymbol{v}$ is positive; therefore, the effect of thermal expansion results in a decrease in the magnitude of vorticity. This can be understood by angular momentum considerations, since as a fluid element expands owing to heat release, the magnitude of its local rotation rate, and hence its vorticity, must decrease to conserve angular momentum.

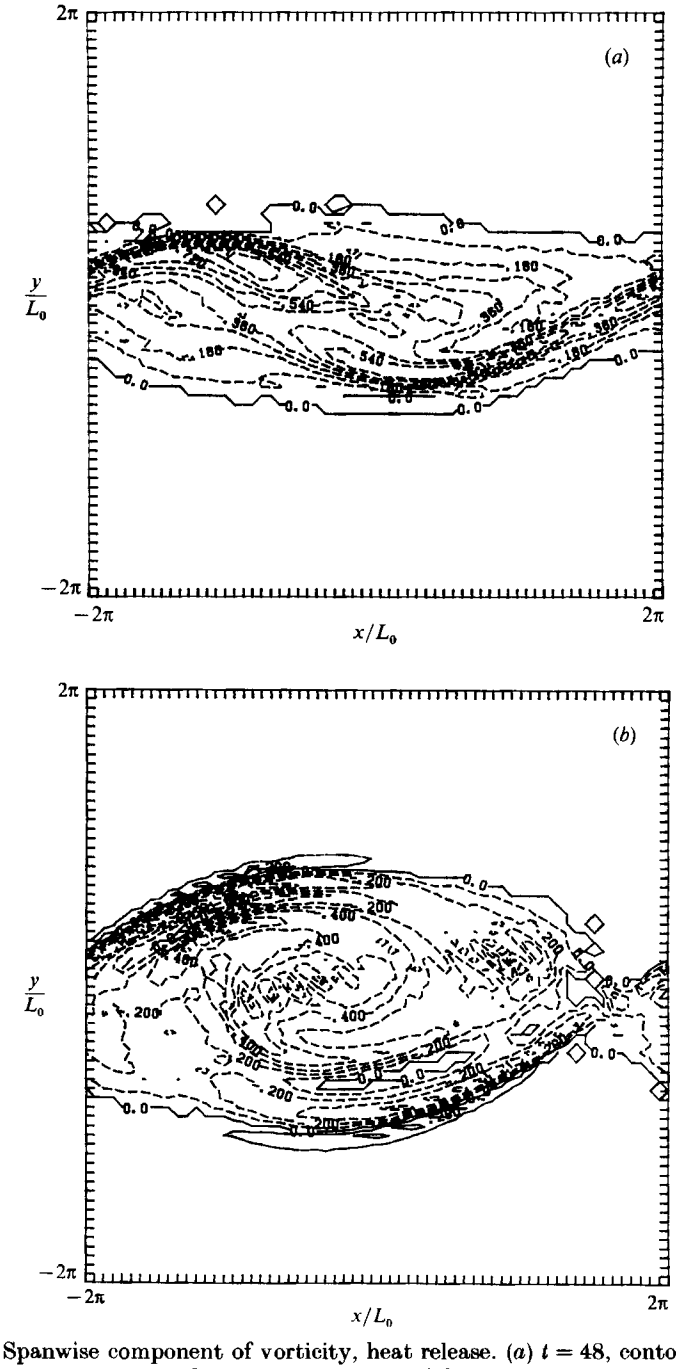

FIGURE 18. Spanwise component of vorticity, heat release. (*a*) $t = 48$, contour level from -0.8 to 0. (*b*) $t = 72$, contour level from -0.7 to 0.2.

The instantaneous value of the spanwise component of the expansion term is shown in figure 19 at two different times. Thermal expansion occurs as heat is released by the chemical reaction, so that this term also gives a good indication of the reaction zone. The rate of reaction is highest where the inflow of reactants into the reaction zone is the highest. This occurs in the regions of highest strain, which are

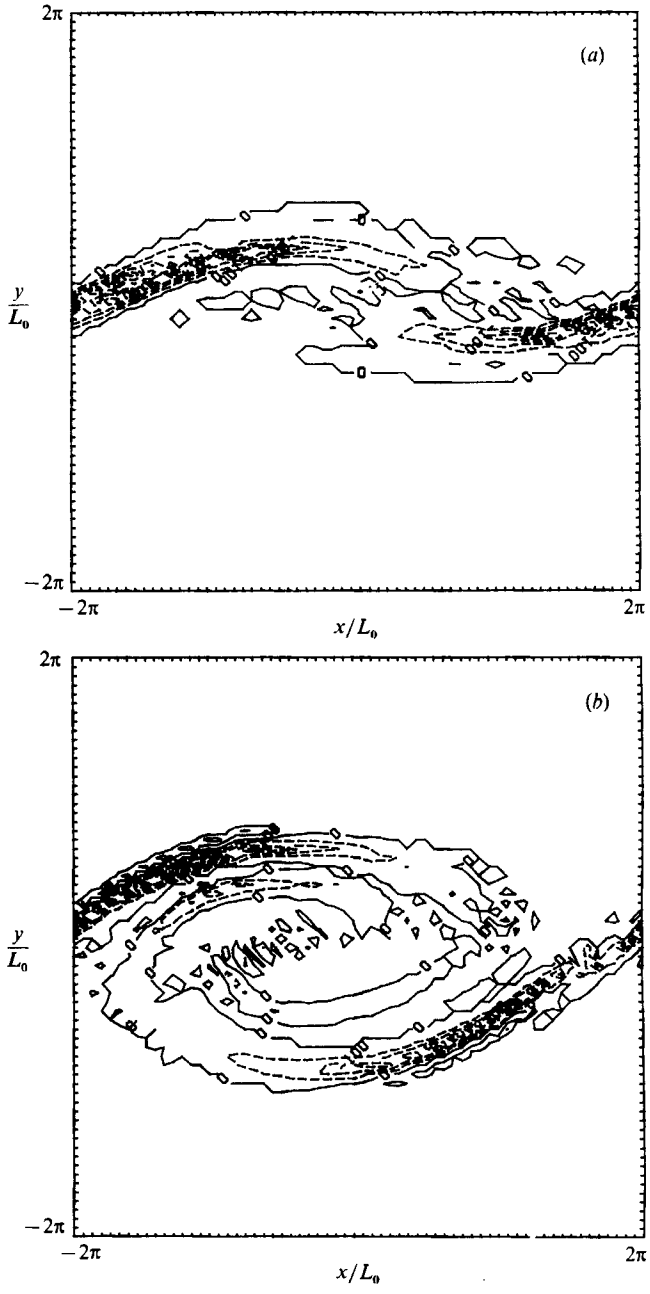

FIGURE 19. Instantaneous value of spanwise component of expansion term in vorticity equation, run 2, spanwise plane $z = 0$. (*a*) $t = 48$, contour level from -0.03 to 0.005. (*b*) $t = 72$, contour level from -0.025 to 0.01.

located in the braids. The result of the expansion is a decrease in the magnitude of vorticity, which in part explains the changes in the vorticity field that result when exothermic chemical reactions occur. (For a temperature-dependent reaction, the high dissipation rates in the braids can cause local quenching of the flame so that the reaction rate is not necessarily highest in the regions where the inflow of reactants is the highest (Peters 1983; Givi *et al.* 1986). This effect is not addressed here.)

The baroclinic torque, $(\nabla\rho \times \nabla p)/\rho^2$ describes differential fluid accelerations resulting from non-aligned pressure gradients. The influence of this term on the flow-field development has been conjectured earlier by Wallace (1981). Using simple geometric relationships between the density and pressure gradients, Wallace reasoned that baroclinic torques may act to reduce entrainment velocities into the mixing layer. The simulation results presented here allow a detailed examination of the actions of this mechanism. Plots of the spanwise component of the baroclinic torque at specific spanwise locations show an alternating sign across the reaction surface and no contribution in the vortex cores (figure 20). This can be understood by recognizing that the density gradient changes sign across the reaction surface, and that the pressure-gradient vector points approximately radially outward from the vortex cores. In the vortex cores the pressure and density gradients are approximately aligned, so there is little contribution of this term here. As the layer rolls up and winds around itself, the baroclinic torque takes on the complicated structure shown in figure 20(*b*), indicating an attempt to generate counter-rotating motions across regions of the reaction zone. Comparisons with the results of two-dimensional simulations show that these effects are dominated by two-dimensional dynamics.

Comparing figures for the spanwise vorticity component (figure 18) and the instantaneous baroclinic torque (figure 20) shows that the regions of positively signed vorticity at the outer regions of the vortices, and also the appearance of multiple extrema in the vorticity field, are a result of the baroclinic torque. The overshoot in the velocity profile seen in the previous section (figure 5) reflects the generation of positive vorticity in this region by the baroclinic torque. This is also possibly the mechanism that produces the previously unexplained inflexion points seen in the velocity profile at the outer edges of jet diffusion flames by Yule *et al.*, and in mixing layers with chemical heat release (M. G. Mungal 1986; J. Hermanson 1986, private communications).

In an attempt to understand the relative importance of the expansion and baroclinic torque on the development of the flow, average values of these two terms are plotted as a function of the height across the mixing layer for a sequence of times (figure 21). (Negative values indicate a decrease in the magnitude of vorticity.) The magnitude of the expansion term is seen to be initially larger than the baroclinic torque term. At later times, the amplitudes of the two terms are comparable. Note that the expansion term consistently produces a net decrease in vorticity. The baroclinic torque tends to decrease the vorticity near the upper and lower limits of the dynamically active region, at least during the initial stages when the two-dimensional modes dominate the flow. This is consistent with the generation of regions of positive vorticity at the edges of the cores (figure 20). Note also that the baroclinic vorticity generation on the centreline is occurring in the braids rather than the cores.

The more diffuse vortex structures which result from the baroclinic torque and thermal expansion lead to a slower rollup of the layer, thus reducing the straining of the reaction interface and decreasing the mass entrainment into the layer. This accounts for much of the decrease seen in the overall product formation and the changes in the layer growth rate. In §7 it was shown (figures 6 and 7) that with heat release, the layer growth rate initially increases, and then decreases compared with the constant-density case. The initial increase was explained to be due to thermal expansion, which tends to shift the whole layer outward. Later in the development of the mixing layer the growth is dominated by the large-scale rollup and pairing

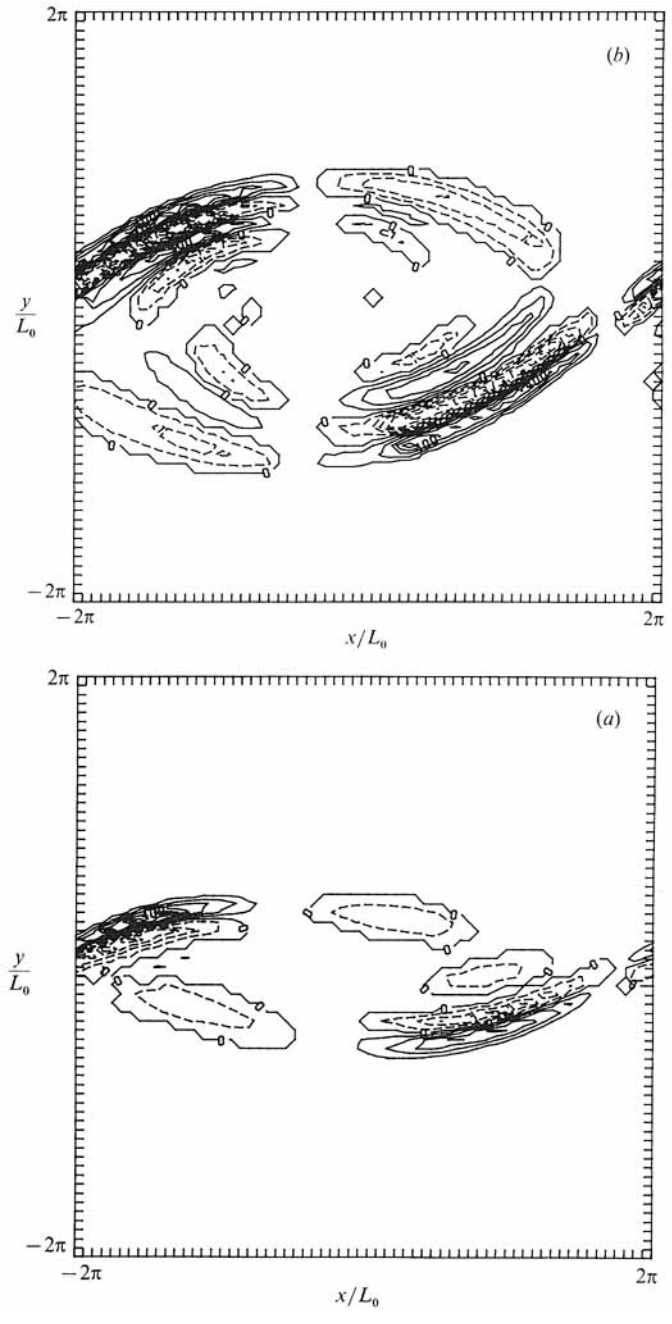

FIGURE 20. Instantaneous value of spanwise component of baroclinic torque, spanwise plane $z = 0$. (*a*) $t = 48$, contour level from -0.04 to 0.06. (*b*) $t = 72$, contour level from -0.05 to 0.05.

processes. Since these processes are inhibited by heat release, the constant-density mixing layer will then grow faster.

The effects of heat release on the three-dimensional, spanwise variation in the reactant concentrations presented earlier can also be interpreted in terms of the vorticity dynamics. Secondary instabilities in the flow are characterized by counter-rotating streamwise vortices (Bernal 1981). The flow field induced by these vortices

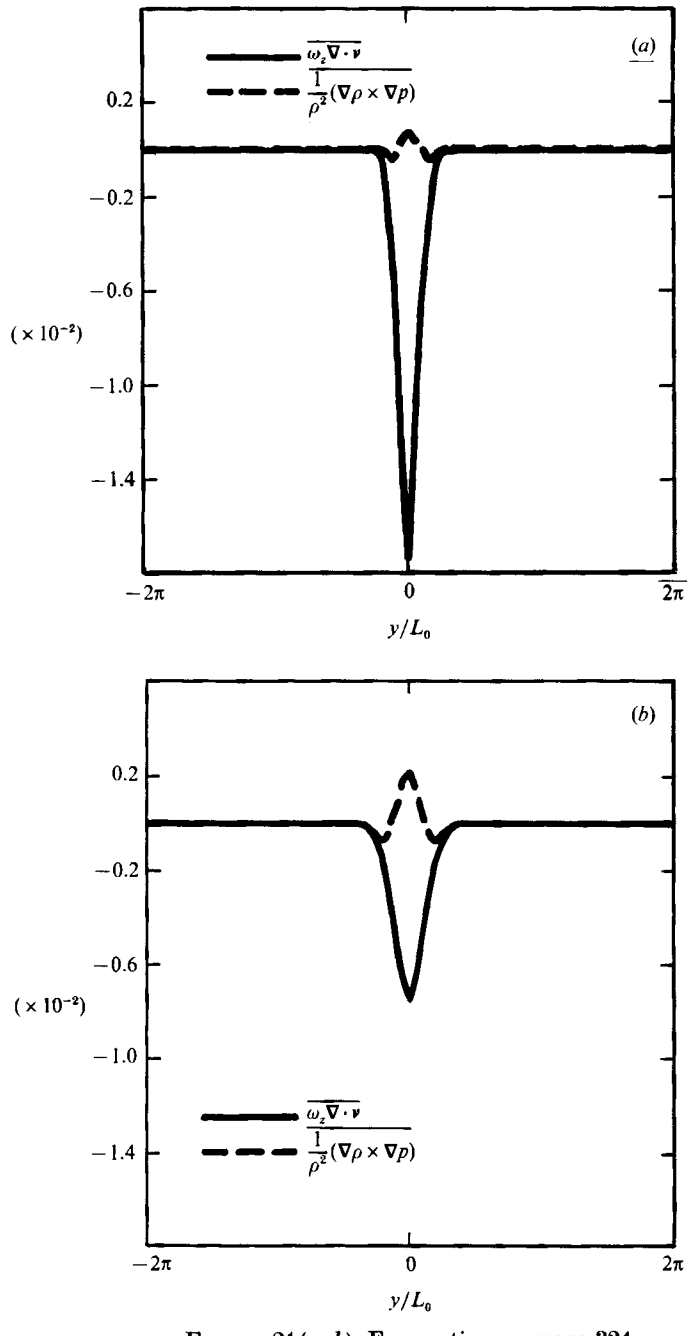

FIGURE 21 (*a*, *b*). For caption see page 324.

enhances mixing and increases the surface area of the interface between the two reacting chemical species, as shown in figure 10(*a*). In figure 22 the streamwise component of vorticity at a time of $t = 72$ is shown in a (y, z)-plane (the mean flow is normal to the figure). Comparing this with a similar plot from run 2 (figure 23) shows a less intense streamwise component of vorticity when heat release accompanies the chemical reaction. The changes seen between these two figures are

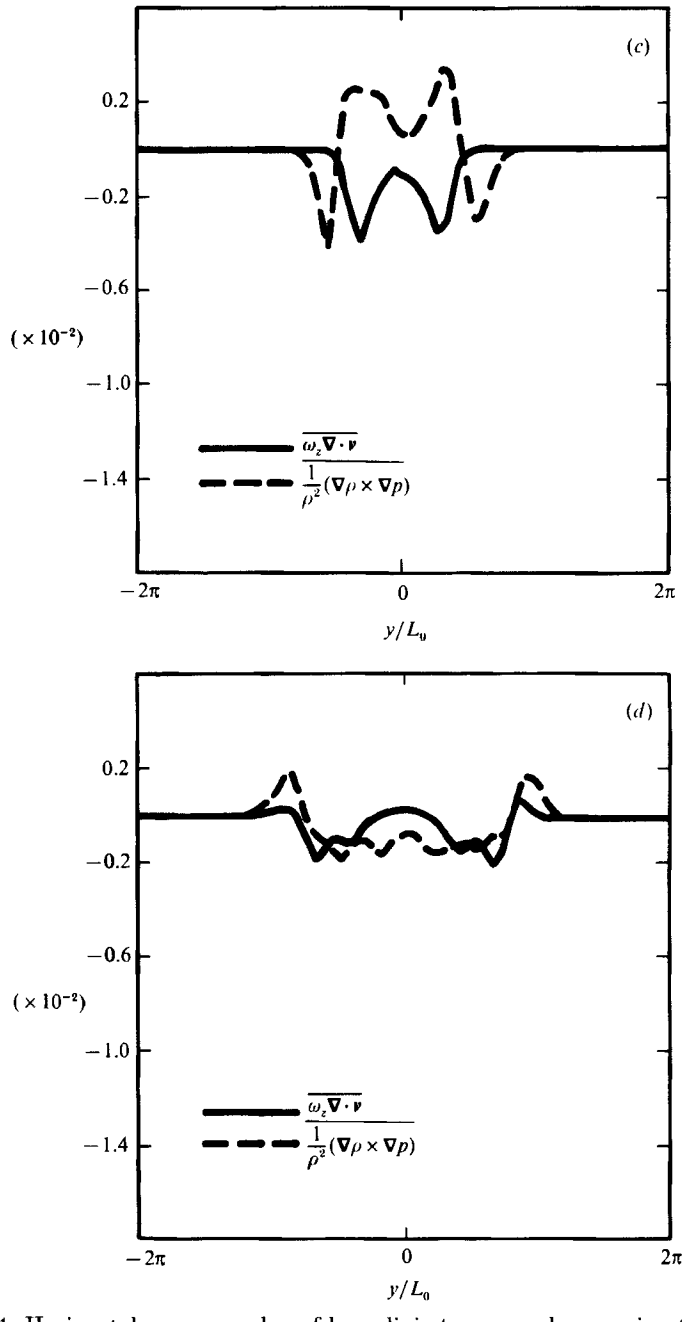

FIGURE 21. Horizontal average value of baroclinic torque and expansion terms transversing the mixing layer. (*a*) $t = 12$, (*b*) 24, (*c*) 48, (*d*) 72.

typical of other streamwise cuts. These structures are subject to alteration by the same mechanisms (baroclinic torques and thermal expansion) as the spanwise vortex structures. In addition, the slower rollup in the heat-release case results in lower strain rates between the spanwise structures, inhibiting streamwise vorticity amplification from vortex stretching. The effect of this on the reactant field is the less wrinkled spanwise variation of the reaction zone as seen in figure 10(*b*).

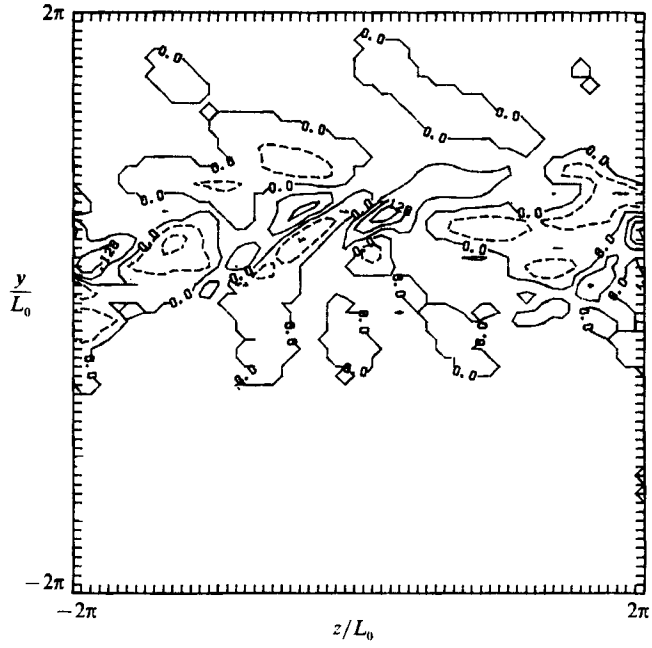

FIGURE 22. Streamwise component of vorticity, (heat release) at one (y, z)-plane, $t = 72$. Contour level from -0.12 to 0.18.

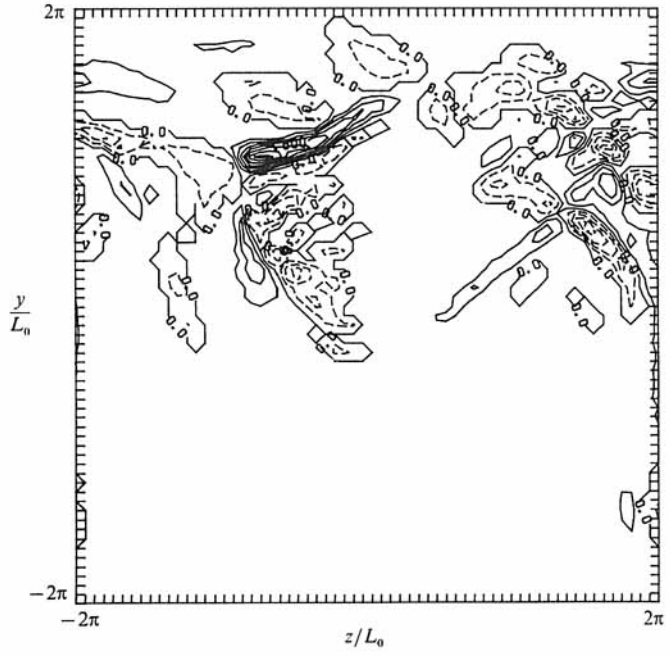

FIGURE 23. Streamwise component of vorticity, (no heat release) at one (y, z)-plane, $t = 72$. Contour level from -0.8 to 1.4.

11. Stability considerations

The question of how the stability characteristics of the mixing layer are affected by heat release is important from both physical and numerical viewpoints. If, as a result of density changes, the unstable modes shift to other wavelengths, or if the growth rates change, this certainly will affect the growth of the mixing layer and the rate at which chemical products are formed. From a computational point of view, it is not possible to look at a continuous distribution of wavelengths. Because of the periodic boundary conditions employed here, only disturbances with wavelengths that divide exactly into the computational domain are allowed (i.e. λ = domain length/n, where n is a positive integer less than the number of modes retained in the simulations). Therefore, if the most unstable modes shift to different wavelengths, dynamically important effects may be overlooked.

To address this question, a linear stability analysis of a simplified model problem was carried out in conjunction with the simulations. This analysis involved a shear layer with a piecewise linear velocity profile with a low density in the velocity transition region (figure 24). The velocity and density in the free stream ($|y| > 1$) were constant, and the density in the transition zone ($|y| < 1$) was also constant and given by $\rho_0(1-\beta)$, where $0 < \beta < 1$. Although this does not exactly describe the conditions in the simulations reported here, the basic characteristics of the two are similar, so that the general trends indicated by the analysis are expected to be true of the simulations. Details of the analysis have been given by McMurtry (1987).

The results of this analysis are plotted in figure 25, which show the growth rate of any individual unstable mode (specified by its wavenumber) for a given value of β. As the density decreases (increasing β), the most unstable mode, represented as the maximum value on each curve, shifts to a lower wavenumber (longer wavelength). The growth rates of the unstable modes are also seen to decrease as the density is lowered, a result consistent with the lower growth rates discussed in §7.

The energy $E(k_x, k_z)$ contained in the two-dimensional modes $k_x = 1$, $k_z = 0$ (this correlates reasonably well with the most unstable two-dimensional mode in the constant-density mixing layer with a hyperbolic mean velocity profile) and $k_x = \frac{1}{2}$, $k_z = 0$ (the subharmonic of the most unstable mode) as a function of time is shown in figures 26 and 27 for runs 1 and 2. This energy is defined as

$$E(k_x, k_z) = \int_{-\infty}^{\infty} |\hat{v}(k_x, k_z, y)|^2 \, \mathrm{d}y,$$

where

$$\hat{v}(k_x, k_z, y) = \sum_{k_y=0}^{N} \hat{u}(k_x, k_z, k_y, t) f(k_y, y).$$

Here $\hat{u}(k, t)$ are the Fourier components of the velocity and $f(k_y, y)$ is either $\sin(k_y y)$ or $\cos(k_y y)$, depending on the component of the velocity under consideration. In the following discussion, we analyse the temporal behaviour of the energies in these Fourier modes.

In figure 26, the energy contained in the fundamental mode ($E_{1,0}$) is compared for runs 1 and 2. For the constant-density case this is the most unstable frequency and is seen to grow until a time of 40, at which point it reaches a quasi-equilibrium, saturated state (Riley & Metcalfe 1980*b*). The behaviour of this mode changes significantly when heat release occurs. The growth drops off at a level well below the incompressible saturation level and at a much earlier time (figure 26), although the initial growth before much density change occurs (up to about $t = 7$) is the same in

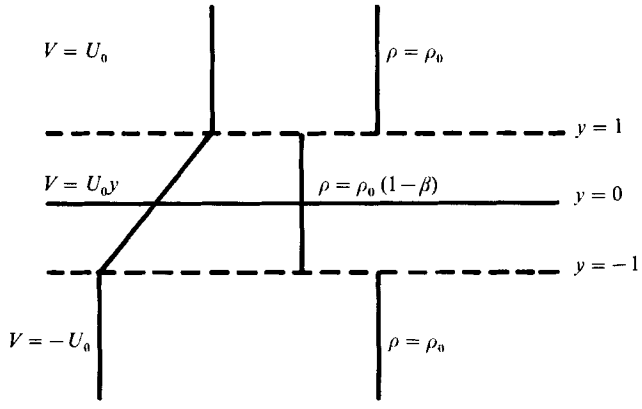

FIGURE 24. Configuration for stability analysis.

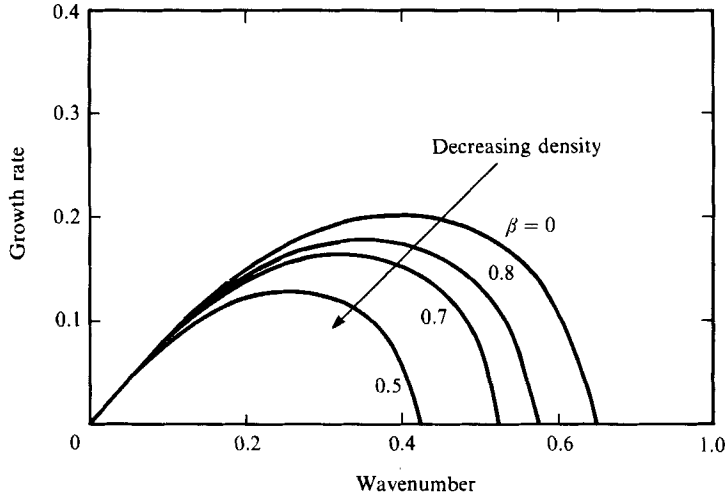

FIGURE 25. Results from linear stability analysis. Growth rates of the unstable modes are plotted for different values of the density (varying β) in the velocity transition region.

the two cases. The subsequent growth of this mode after $t = 30$ is due to its growth as a component of the subharmonic mode. The energy in the subharmonic ($E_{\frac{1}{2},0}$) increases until it reaches its saturation level at a time of 65 in the constant-density case (figure 27). The subharmonic remains unstable with the addition of heat to the flow, but grows at a slower rate than in the constant-density case. The energy in the three-dimensional modes (the sum of $E(k_x, k_z)$ for all k_x and $k_z \neq 0$) is also seen to be less for the heat release run, as shown in figure 28.

The results of the simplified linear analysis for the linear profiles compare favourably with the simulation results. The density changes occurring in run 2 correspond to a β of 0.5. With this amount of heat release, the most unstable mode in the constant-density case is predicted to be stable, which is consistent with the model behaviour in the simulations (figure 26). From the stability analysis, the actual most unstable mode shifts to the wavenumber corresponding to that of the subharmonic of the most unstable mode in the constant-density case (0.22). From figure 27, the growth rate ($E^{-1}\partial E/\partial t$) of the subharmonic is shown to decrease from

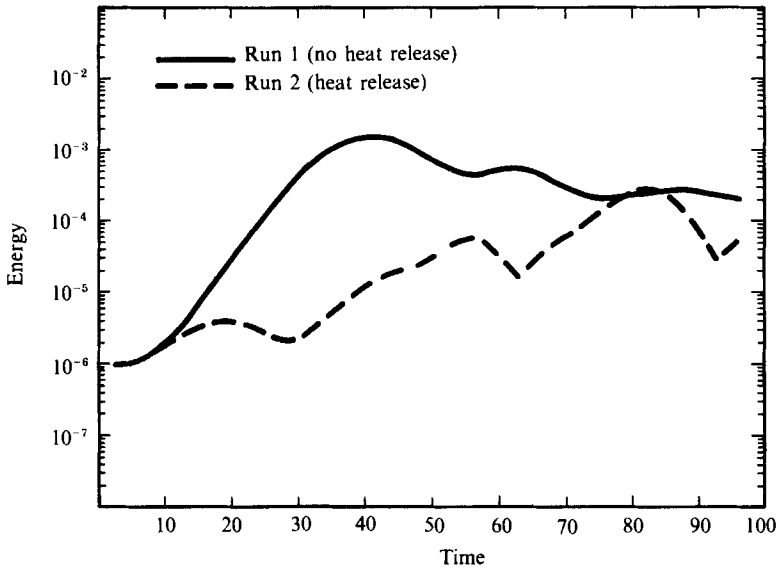

FIGURE 26. Comparison of energy in fundamental mode, with and without heat release.

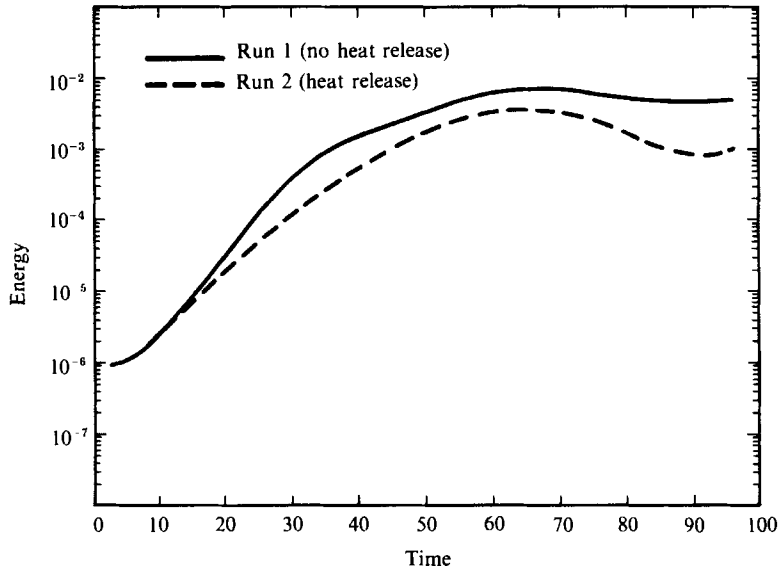

FIGURE 27. Comparison of energy in subharmonic, with and without heat release.

0.18 to 0.13, while in the simulations the computed growth rate of the subharmonic decreased from 0.12 to 0.09 in the heat-release case. In figure 28 this lower growth rate of the subharmonic is indicated by the smaller slope.

The laboratory experiments on mixing layers, which clearly show lower growth rates of the mixing layer as heat release is increased, do not lead to any firm conclusions regarding the suppression of modes or a shift in the wavelengths of the most unstable modes. Although the experiments performed by Hermanson (1985) appear to indicate a slight decrease in the spacing (wavelengths) between the vortex

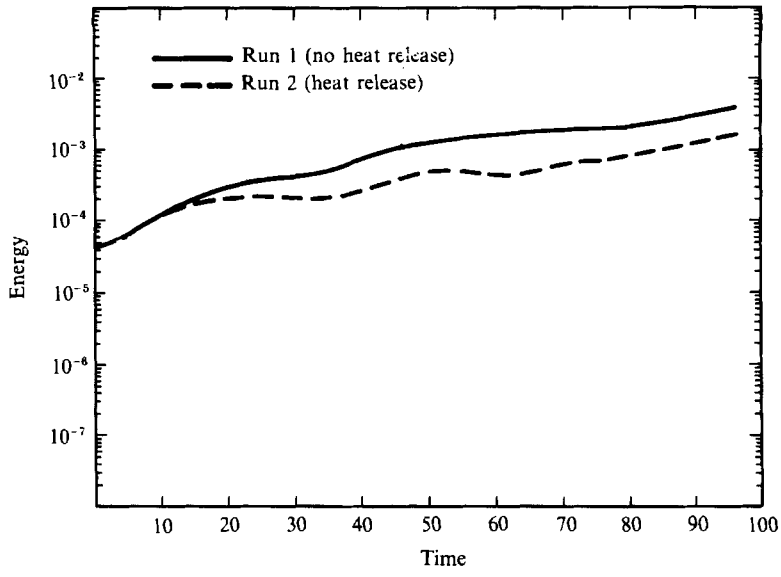

FIGURE 28. Comparison of energy in three-dimensional modes with and without heat release.

cores when heat release occurs, this observation alone does not confirm or contradict the possibility that the frequencies of the unstable modes are shifted to longer wavelengths by heat release. In particular, if the heat release acts to eliminate only the highest-wavenumber components as suggested in the previous analysis (figure 25), this would only be seen in the near field of the splitter plate. If the growth rates of lower modes are also inhibited, as suggested by the analysis presented here, this would delay pairing of adjacent structures, resulting in an apparent decrease in the spacing between cortex cores. A distinct suppression of modes and a change in the wavelengths of the unstable modes has been observed, however, in experiments on jet flames. Schlieren photographs of the near nozzle region by Savaş & Gollahalli (1986) and Gollahalli *et al.* (1986) show that the presence of flames substantially suppresses the formation and development of both organized structures and secondary azimuthal instabilities. Measurements by Yule *et al.* (1981) show the frequencies of the most energetic modes decrease as heat release is increased, a result consistent with the simulations and analysis presented here.

12. Summary

The simulation results discussed here and related laboratory experiments have shown that, when heat release accompanies chemical reaction, the mixing layer grows at a lower rate and the amount of product formed decreases. In addition, an overshoot in the velocity profile appears. A study of the flow in terms of vorticity dynamics explored two mechanisms that do not act in constant-density flows: the baroclinic torque and thermal expansion. The action of these mechanisms was shown to result in more diffuse vortices when heat release accompanies the chemical reaction. For higher rates of heat release it may be expected that the baroclinic generation of vorticity may produce stronger counter-rotating eddies at the outer regions of the large-scale spanwise structures and become a more important mechanism for enhanced mixing in the shear layer. At the largest scales (which

dominate the dynamics of the flow and account for most of the turbulent transport), the altered vorticity distribution resulted in slower rollup of the most unstable modes, giving lower growth rates and less entrainment of unmixed fluid. This was indicated by the lower energies and growth rates of the unstable modes computed in the simulations and confirmed by a stability analysis of a simplified model problem similar to the mixing-layer flow simulated here. The appearance of 'humps' in the velocity profile were shown to be the result of vorticity generation in the outer regions of the spanwise vortices by baroclinic torques.

The turbulent kinetic energy and the turbulent shear stresses are closely related, since the turbulent stresses are a direct indication of the kinetic energy transfer from the mean flow to or from the turbulence. Lower values of both the turbulent kinetic energy and the turbulent stresses were observed in the heat release runs. This can be related directly to the vorticity dynamics by realizing that in turbulent flows, the largest eddies (vortices) are responsible for most of the transport of momentum and scalar quantities. The weaker large-scale vortices that result when heat release occurs transport less momentum, which is exactly what the lower values of the turbulent shear stresses indicate. The transport rates of the chemical reactants will also result in less product formation, as observed in the simulations and laboratory experiments.

This study has benefitted from numerous suggestions and ideas generously provided by Dr W.-H. Jou. This work was supported in part by the NASA Lewis Research Center under contract NAS3-24229 to Flow Industries, Inc., and by ONR Contract No. N00014-87-K-0174 to the University of Washington. All computer simulations were performed on the CRAY X-MP at the NASA Lewis Research Center. The encouragement given from Mr Russ Claus of NASA Lewis Research Center in pursuing this research is greatly appreciated.

REFERENCES

ACTON, E. 1976 The modelling of large eddies in a two-dimensional shear layer. *J. Fluid Mech.* **76**, 561–592.

AREF, A. & SIGGIA, E. D. 1980 Vortex dynamics of the two-dimensional turbulent shear layer. *J. Fluid Mech.* **100**, 53–95.

ASHURST, W. T. & MEIBERG, E. 1988 Three-dimensional shear layers via vortex dynamics. *J. Fluid Mech.* **189**, 87–110.

BERNAL, L. P. 1981 The coherent structure of turbulent mixing layers. I. Similarity of the primary vortex structures. II. Secondary streamwise vortex structure. Ph.D. thesis, California Institute of Technology.

BREIDENTHAL, R. E. 1981 Structure in turbulent mixing layers and wakes using a chemical reaction. *J. Fluid Mech.* **109**, 1–24.

BROWN, G. L. & ROSHKO, A. 1974 On density effects and large structure in turbulent mixing layers. *J. Fluid Mech.* **91**, 319–335.

BUCKMASTER, J. D. 1985 An introduction to combustion theory. In *The Mathematics of Combustion.* (ed. J. Buckmaster), pp. 3–46. SIAM.

CANUTO, C., HUSSAINI, M. Y., QUARTERONI, A. & ZANG, T. A. 1988 *Spectral Methods in Fluid Dynamics.* Springer.

CORCOS, G. M. & SHERMAN, F. S. 1984 The mixing layer: deterministic models of a turbulent flow. Part 1. Introduction and the two-dimensional flow. *J. Fluid Mech.* **139**, 29–65.

DIMOTAKIS, P. E. 1986 Entrainment and growth of a fully developed, two-dimensional shear layer. *AIAA J.* **24**, 1791–1796.

GIVI, P., JOU, W.-H. & METCALFE, R. W. 1986 Flame extinction in a temporally developing mixing layer. *Twenty-first Symp. (Intl) on Combustion*, pp. 1251–1261. The Combustion Institute.

GOLLAHALLI, S. R., SAVAŞ, Ö., HUANG, R. F. & AZARA, J. L. R. 1986 Structure of attached and lifted gas jet flames in hysteresis region. In *Twenty-first Symp. (Intl) on Combustion*, pp. 1463–1471. The Combustion Institute.

GOTTLIEB, D. & ORSZAG, S. A. 1977 *Numerical Analysis of Spectral Methods*. Philadelphia: SIAM.

HERMANSON, J. C. 1985 Heat release effects in a turbulent shear layer. Ph.D. thesis, California Institute of Technology.

HOTTEL, H. C. & HAWTHORNE, W. R. 1953 In *Third Symp. (Intl) on Combustion*, p. 254. Williams and Wilkens.

JOU, W. H. & RILEY, J. J. 1989 Progress in direct numerical simulations of turbulent reacting flows. *AIAA J.* (to appear). Also *AIAA paper* 87–1324.

KARAGOZIAN, A. 1982 An analytical study of diffusion flames in vortex structures. Ph.D. thesis, California Institute of Technology.

KELLER, J. O. & DAILY, J. W. 1985 The effects of highly exothermic chemical reaction on a two-dimensional mixing layer. *AIAA J.* **23**, 1937–1945.

KONRAD, J. H. 1976 An experimental investigation of mixing in two-dimensional turbulent shear flows with application to diffusion limited chemical reactions. Ph.D. thesis, California Institute of Technology.

KOOCHESFAHANI, M. M. 1984 Experiments on turbulent mixing and chemical reactions in a liquid mixing layer. Ph.D. thesis, California Institute of Technology.

LASHERAS, J. C., CHO, J. S. & MAXWORTHY, T. 1986 On the origin and evolution of streamwise vortical structures in a plane, free shear layer. *J. Fluid Mech.* **172**, 231–258.

LIBBY, P. A. & WILLIAMS, F. A. 1980 Fundamental aspects of turbulent reacting flows. In *Turbulent Reacting Flows* (ed. P. A. Libby & F. A. Williams), pp. 1–43. Springer.

LIN, S. J. & CORCOS, G. M. 1984 The mixing layer deterministic models of a turbulent flow. Part 3. The effect of plain strain on the dynamics of streamwise vortices. *J. Fluid Mech.* **141**, 139–178.

LOWREY, P. S. & REYNOLDS, W. C. 1986 Numerical simulation of a spatially-developing, forced, plane mixing layer. *Rep.* TF-26. Department of Mechanical Engineering, Stanford University.

MAJDA, A. & SETHIAN, J. 1985 The derivation and numerical solution of the equations for zero Mach number combustion. *Combust. Sci. Tech.* **42**, 185–205.

MARBLE, F. E. & BROADWELL, J. E. 1977 The coherent flame model of turbulent chemical reactions. *Project SQUID Tech. Rep.* TRW-9-PU.

MASUTANI, S. M. 1985 An experimental investigation of mixing and chemical reaction in a plane mixing layer. Ph.D. thesis, Stanford University.

MCMURTRY, P. A. 1987 Direct numerical simulations of a reacting mixing layer with chemical heat release. Ph.D. thesis, University of Washington.

MCMURTRY, P. A., JOU, W.-H., RILEY, J. J. & METCALFE, R. W. 1986 Direct numerical simulations of a reacting mixing layer with chemical heat release. *AIAA J.* **24**, 962–970.

METCALFE, R. W., ORSZAG, S. A., BRACHET, M. E., MENON, S. & RILEY, J. J. 1987 Secondary instability of a temporally growing mixing layer. *J. Fluid Mech.* **184**, 207–243.

MICHALKE, A. 1964 On the inviscid instability of the hyperbolic tangent velocity profile. *J. Fluid Mech.* **19**, 543–556.

MUNGAL, M. G. & DIMOTAKIS, P. E. 1984 Mixing and combustion with low heat release in a turbulent shear layer. *J. Fluid Mech.* **148**, 349–382.

ORSZAG, S. A. & PAO, Y. 1974 Numerical computation of turbulent shear flows. *Adv. Geophys.* **18**, 225–236.

ORSZAG, S. A. & PATTERSON, G. S. 1972 Numerical simulation of turbulence. In *Statistical Models and Turbulence* (ed. M. Rosenblatt & C. Van Atta). Lecture Notes in Physics, vol. 12, pp. 127–147. Springer.

PATNAIK, P. C., SHERMAN, F. S. & CORCOS, G. M. 1976 A numerical simulation of Kelvin–Helmholtz waves of finite amplitude. *J. Fluid Mech.* **73**, 215–240.

PETERS, N. 1983 Local quenching due to flame stretching and non-premixed turbulent combustion. *Combust. Sci. Tech.* **30**, 1–17.

PIERREHUMBERT, R. T. & WIDNALL, S. E. 1982 The two- and three-dimensional instabilities of a spatially periodic shear layer. *J. Fluid Mech.* **114**, 59–82.

REHM, R. G. & BAUM, H. R. 1978 The equations of motion for thermally driven, buoyant flows. *Natl. Bur. Stand. J. Res.* **83**, 297–308.

RILEY, J. J. & METCALFE, R. W. 1980*a* Direct numerical simulations of the turbulent wake of an axisymmetric body. In *Turbulent Shear Flows II* (ed. L. S. Bradbury, F. Durst, B. E. Launder, F. W. Schmidt & J. H. Whitelaw), pp. 78–93. Springer.

RILEY, J. J. & METCALFE, R. W. 1980*b* Direct numerical simulations of a perturbed, turbulent mixing layer. *AIAA Paper* 80-0274.

RILEY, J. J. & METCALFE, R. W. & ORSZAG, S. A. 1986 Direct numerical simulations of chemically reacting mixing layers. *Phys. Fluids* **29**, 406–422.

ROGALLO, R. W. & MOIN, P. 1984 Numerical simulation of turbulent flows. *Ann. Rev. Fluid Mech.* **16**, 99–137.

SAVAŞ, Ö. & GOLLAHALLI, S. R. 1986 Flow structure in near-nozzle region of gas jet flames. *AIAA J.* **24**, 1137–1140.

SIVASHINSKY, G. O. 1979 Hydrodynamic theory of flame propagation in an enclosed volume. *Acta Astronaut.* **6**, 631–645.

TAKAGI, T., SHIN, H.-D. & ISHIO, A. 1980 Local laminarization in turbulent diffusion flames. *Combust. Flame* **37**, 163–170.

TAKENO, T. & KOTANI, Y. 1975 An experimental study on the stability of jet diffusion flames. *Acta Astronaut.* **2**, 999–1008.

WALLACE, A. K. 1981 Experimental investigation on the effects of chemical heat release on shear layer growth and entrainment. Ph.D. thesis, University of Adelaide.

WHOL, K., GAZLEY, C. & KAPP, A. J. 1949 Diffusion Flames. In *Third Symp. on Combustion Flame and Combustion Phenomena*, pp. 288–300. Combustion Institute, Pittsburgh, Pa.

WINANT, C. D. & BROWAND, F. K. 1974 Vortex pairing, the mechanism of turbulent mixing-layer growth at moderate Reynolds number. *J. Fluid Mech.* **63**, 237–255.

YULE, A. J., CHIGIER, N. A., RALPH, S., BOULDERSTONE, R. & VENTURA, J. 1981 Combustion-transition interaction in a jet flame. *AIAA J.* **19**, 752–760.